

Pulse area theorem in optical waveguide and its application to photon echo

S.A. Moiseev^{1*} and M.M. Minnegaliev¹, A.V. Pavlov¹, K.I. Gerasimov¹,
E.S. Moiseev¹, T.A. Rupasov¹, N.N. Skryabin², A.A. Kalinkin², S.P. Kulik^{2,3}
¹*Kazan Quantum Center, Kazan National Research Technical University*
n.a. A.N. Tupolev-KAI, 10 K. Marx St., 420111, Kazan, Russia

²*Quantum Technologies Center and Faculty of Physics,*

M.V. Lomonosov Moscow State University, Leninskie Gory, 119991, Moscow, Russia and

³*Laboratory of quantum engineering of light, South Ural State University (SUSU), Lenin Avenue, 454080, Chelyabinsk, Russia*

(Dated: October 21, 2022)

We derive the area theorem for light pulses resonantly interacting with atoms in a single-mode optical waveguide and present its analytical solution for Gaussian-type modes, which demonstrates the significant difference from the formation of 2π pulses by plane waves. We generalize this theorem to the description of photon echo and apply it to the two-pulse (primary) echo and the revival of silenced echo (ROSE) protocol of photon echo quantum memory. For the first time, we implemented ROSE protocol in a single-mode laser-written waveguide made of an optically thin crystal $\text{Tm}^{3+}:\text{Y}_3\text{Al}_5\text{O}_{12}$. The experimental data obtained are satisfactorily explained by the developed theory. Finally, we discuss the experimental results obtained and possible applications of the derived pulse area approach.

I. INTRODUCTION

Coherent interaction of light pulse with resonant atomic ensembles plays a significant role in modern optics and quantum technologies [1–4]. It was found that pulse area theorem [5] provides simple but powerful tool for general analysis of coherent light-atoms dynamics in self-induced transparency [5], optical solitons [6], super-radiance [7], photon echo in optically dense media [8–10] to name a few. The approach was developed for plane light waves propagating and interacting with atoms in free space. Recent progress in integrated quantum photonics [11–14] pushes study of the coherent interaction between light pulse and resonant atomic ensembles in optical waveguides, where the development of waveguide optical quantum memory (QM) is attracting growing attention [15–20].

Optical QM is designed to provide storage of quantum states of light with subsequent retrieval of these states on demand at an arbitrary time [21–26]. QM is a vital component for numerous quantum technologies such as long-distance quantum communications [4, 27, 28], quantum state preparation [29], synchronization unit for optical quantum processing [24]. Currently, there is growing interest in the implementation of optical QM in optical waveguides [16, 18, 30–32] doped with rare-earth ions (REI) which seem as a convenient platform for implementation of on-chip QM. Quantum storage in REI-doped waveguides was demonstrated in experiments on heralded single photon storage [33, 34], on-demand qubit storage [35] and frequency-multiplexed storage [36].

All of the above experiments are based on the scheme of reversible photon echo in an optically dense medium [37, 38], realized for inhomogeneous broadening in the

form of a periodic narrow atomic frequency comb that is called AFC-protocol [39]. Typical AFC structure is created by laser hole-burning technique [40], which leads to a strong decrease in optical density and corresponding decrease in the efficiency of the AFC protocol to 10-30% [41–43]. For higher values of efficiency and fidelity of the AFC protocol, either its spectral structure must be modified to ensure zero spectral dispersion in the operating frequency range [44, 45] or AFC-medium should be placed in an optical resonator [46, 47], where the requirement to use a high optical density of the atomic transition is removed. The use of optical waveguides could be another alternative, where it is also possible to significantly enhance the interaction of atoms with waveguide modes, although it is apparently impossible to achieve as much enhancement as in a resonator.

At the same time, the use of waveguides is especially relevant for combining QM cells with optical integrated circuits. The problem of achieving high efficiency can be solved by using other QM protocols, e.g. revival of silent echo (ROSE) protocol [48, 49], which is the closest modification of the two-pulse photon echo. In this case, it is possible to use a naturally inhomogeneous broadened resonant transition with recalled of stored pulses being controlled by two π -pulses. Such control pulses are also used in other photon echo QM protocols [23, 26]. The mentioned need for a highly efficient implementation of photon echo QMs and its integration with waveguide schemes makes it relevant to develop a general theoretical approach for describing the coherent interaction of light with atoms in optical waveguides. The approach should properly simulate the application intense control laser fields, e.g. π -pulses, that induce nonlinear dynamics of resonant atoms.

Since the McCall-Hahn work [5], it was discovered that the most general patterns of linear and nonlinear interaction of light pulses with coherent two-level media can be described by the area theorem [6, 7]. The area theorem

* s.a.moiseev@kazanqc.org

was applied to the description of photon echo in optically dense media [8, 9, 50, 51] and in Fabry-Perot resonator [10] as well as it was applied for studies of photon echo CRIB protocol in free space [52] and for description of experimental results of cavity assistant ROSE protocol [53]. It is worth noting that in recent experiments [51, 53], it has been found that in media with a symmetrical form of inhomogeneous broadening, the behavior of the pulse area of the echo signal almost flatly reproduces the behavior of the amplitude of echo signals. It makes this approach universal for describing linear and nonlinear behaviour in various scenario of photon echo, as well as QM protocols based on this effect in optically dense resonant media.

In this work, we derive the pulse area theorem for the resonant interaction of a light pulse with two-level atoms in a single-mode optical waveguide (W-pulse area theorem). We found the analytical solution of the W-pulse area theorem, demonstrating significant differences in the conditions for the formation of stable 2π pulses compared to the well-known McCall-Hahn pulse area theorem [5]. Then we generalize W-pulse area theorem for the echo signal emission and apply it for description of the two-pulse (primary) photon echo, ROSE-protocol of photon echo QM. For the first time, we present experimental results on ROSE protocol in a laser-written waveguide of a Tm^{3+} crystal: $\text{Y}_3\text{Al}_5\text{O}_{12}$. Then we discuss the obtained experimental data using W-pulse area theorem and focusing on the factors leading to negative impact on the efficiency of the QM protocol implementation and outline the possible applications of the developed theoretical approach to other problems.

II. W-PULSE AREA THEOREM

A. Basic equations

We consider the interaction of a light pulse with a system of atoms in a single-mode waveguide, where the basic interaction includes the Hamiltonian of waveguide light modes H_f , two-level atomic ensemble with inhomogeneous broadening H_a and the dipole interaction of atoms with light modes V_{fa} . To describe the losses in the waveguide in the total Hamiltonian $H = H_f + H_a + H_b + V_{ba} + V_{fb}$ we also include the Hamiltonian of the local bath modes H_b and their interaction with the modes of the light field V_{fb} ; $H_f = \hbar \int dz a^\dagger(z) [\omega a(z) - i v_g \frac{\partial}{\partial z} a(z)]$ [54], where $v_g = \frac{\partial \omega}{\partial \beta}$ - group velocity, $\beta = \sqrt{k^2 - (2\pi/\Lambda)^2}$, $k = n(\omega)\omega/c$, Λ is a critical waveguide wavelength [55], $H_a = \sum_{m=1}^M \sum_{j=1}^{N_m} \frac{1}{2} \hbar (\omega + \Delta_j) \sigma_{3,m}^j$ (N_m is a number of atoms with dipole moment \mathbf{d}_m) and $H_b = \hbar \sum_{n=1}^{N_w} \int d\omega_n \omega_n \hat{b}^\dagger(\omega_n) \hat{b}(\omega_n)$; Hamiltonians of the interaction between field modes with resonant atoms V_{fa} and with bath modes V_{fb} are: $V_{af} = -\frac{1}{2} \hbar \sum_m \sum_j^{N_m} \Omega_{0,m}(\mathbf{r}_\perp^j) \sigma_{-,m}^j \hat{a}^\dagger(z_j) e^{-ikz_j} + h.c.$, $V_{fb} =$

$\hbar \sum_n f_n \hat{a}^\dagger(z_n) e^{-i\beta z_n} \hat{B}_n + h.c.$ (where $\hat{B}_n = \int d\omega_n \hat{b}(\omega_n)$, f_n - coupling constant of field mode with bath modes at z_n , below we assume $f_n = f$ for simplicity); the electric field of light field in the waveguide is given by the operator:

$$\hat{\mathbf{E}}(\mathbf{r}, t) = \mathbf{e} E_0 f(\mathbf{r}_\perp) \hat{a}_0^\dagger(z, t) e^{i\omega t - i\beta z} + h.c., \quad (1)$$

where $E_0 f(\mathbf{r}_\perp)$ is single photon electric field amplitude in single mode waveguide [2], $f(\mathbf{r}_\perp)$ - membrane function [55]. \mathbf{e} is a polarization vector, $\hat{a}_0(z, t) = \hat{a}(z, t) e^{i\omega t - i\beta z}$ ($\hat{a}_0^\dagger(z, t) = (a_0(z, t))^\dagger$) is slowly varying bosonic annihilation (creation) operator of light field mode at given coordinate z with commutation relationship $[\hat{a}_0(z, t), \hat{a}_0^\dagger(z', t)] = \delta(z - z')$, index 0 = s; e for signal and echo fields.

Using the introduced Hamiltonian, the dynamics of quantum light interacting with two-level media is described by the Heisenberg-Langevin equations [2, 56]:

$$\left(\frac{\partial}{\partial t} + \frac{\gamma_w}{2} + v_g \frac{\partial}{\partial z} \right) \hat{a}_0(z, t) = \frac{i}{2} \sum_{m=1}^M \sum_{j=1}^{N_m} \Omega_{0,m}(\mathbf{r}_\perp^j) \hat{\sigma}_{-,m}^j(t) \delta(z - z_j) + \sqrt{\gamma_w} \hat{b}_{in}(z, t), \quad (2)$$

where $\Omega_{0,m}(\mathbf{r}_\perp^j) = E_0 f(\mathbf{r}_\perp^j) \langle \mathbf{d}_m \cdot \mathbf{e} \rangle / \hbar$ is a single photon Rabi-frequency for an atom located for j-th atom located at $\mathbf{r}^j = \mathbf{r}_\perp^j + z_j \mathbf{e}_z$, $\gamma_w = 2\pi^2 |f|^2 \rho$ - the losses rate of waveguide modes due to scattering on the irregularities of the waveguide walls ($\rho = N_w/L$, L - length of the waveguide) and noise field operator related to these losses $\hat{b}_{in}(z, t) = -i \sqrt{\frac{2\pi}{\gamma_w}} f^* \sum_n \hat{B}_n(t_0 \rightarrow -\infty) e^{-i(\omega_n - \omega)(t - t_0)} \delta(z - z_n)$ ($\langle \hat{b}_{in}(z, t) \rangle = 0$, $[\hat{b}_{in}(z, t) \hat{b}_{in}^\dagger(z', t')] = \delta(z - z') \delta(t - t')$). The same atom isospin flip operators $\sigma_{-,+}^j$ are introduced, such that $\sigma_{\pm}^j = (\sigma_1^j \pm i\sigma_2^j)/2$ with $\sigma_1^j, \sigma_2^j, \sigma_3^j$ being standard set of Pauli matrices, N_m - number of atoms in m-th group.

The dependence of $\Omega_{0,m}(\mathbf{r}_\perp^j)$ on the spatial position of the atom is determined by the structure of the electric field of the light mode in the cross-section of the waveguide. We assume it as a real value for the considered modes. The local operators $\hat{b}_{in}(z, t)$ and decay term $\frac{\gamma_w}{2} \hat{a}_0(z, t)$ were derived following the quantum optics input-output formalism [56]. These operators describe the light decay in the waveguide and Langevin forces in the continuous medium, where $\hat{b}_{in}(z, t)$ is determined by the input local fields $\hat{b}(\omega_n, t_0 \rightarrow -\infty)$. Therefore, by introducing local noise operators $\hat{b}_{out}(z, t)$ at $t_0 \rightarrow \infty$, we get the following local relation similar to resonator input-output approach [56]:

$$\hat{b}_{in}(z, t) - \hat{b}_{out}(z, t) = \sqrt{\gamma_w} \hat{a}_0(z, t). \quad (3)$$

The relation (3) is useful for describing the absorption of a light pulse and can be used to consider echo signals. Together with field equation (2), we similarly derive Heisenberg-Langevin equations for the resonant atoms [2]:

$$\begin{aligned} \frac{\partial \sigma_{-,m}^j}{\partial t} = & -(\gamma/2 + i\Delta_j)\sigma_{-,m}^j \\ & - i\Omega_{0,m}(\mathbf{r}_\perp^j)\hat{a}_0(z_j, t)\sigma_{3,m}^j + \sqrt{\gamma}\hat{F}_{j,m}, \end{aligned} \quad (4)$$

$$\begin{aligned} \frac{\partial \sigma_{+,m}^j}{\partial t} = & -(\gamma/2 - i\Delta_j)\sigma_{+,m}^j \\ & + i\Omega_{0,m}(\mathbf{r}_\perp^j)\hat{a}_0^\dagger(z_j, t)\sigma_{3,m}^j + \sqrt{\gamma}\hat{F}_{j,m}^\dagger, \end{aligned} \quad (5)$$

$$\frac{\partial \sigma_{3,m}^j}{\partial t} = -2i\Omega_{0,m}(\mathbf{r}_\perp^j) \left[\hat{a}_0^\dagger(z_j, t)\sigma_{-,m}^j - \hat{a}_0(z_j, t)\sigma_{+,m}^j \right]. \quad (6)$$

The (4)-(6) for j -th atom include pure dephasing γ with related atomic Langevin forces $\hat{F}_{j,m}(t), \hat{F}_{j,m}^\dagger(t)$ (where $\langle \hat{F}_j(t)\hat{F}_j^\dagger(t') \rangle = \delta_{j,j'}\delta(t-t')$) that are assumed identical for all atoms, $\Delta_j(t) = \Delta_j + \delta\Delta_j(t)$, Δ_j and $\delta\Delta_j(t)$ are the static and fluctuating frequency offsets of j -th atom, where Δ_j are inhomogeneously broadened by spectral distribution $G(\frac{\Delta}{\Delta_{in}})$ with spectral width Δ_{in} [1]. Eqs. (2)-(6) should be solved for the stages of storage and retrieval of quantum signal fields. Below we are only focusing on consideration of classical light fields, passing from field operators $\hat{a}_m(z, t)$ to classical real values $a_p(z, t) = \langle \hat{a}_p(z, t) \rangle = \langle \hat{a}_p^\dagger(z, t) \rangle$ ($p = s; c; 0$ index indicating signal, control and echo pulses) and omitting the Langevin forces ($\langle \hat{b}_{in}(z, t) \rangle = 0$). Note that the classical equation for the electromagnetic field obtained in this case, although it does not allow describing the purely quantum properties of light, can describe the interaction of single-photon light fields with resonant atoms and is suitable for the analysis of optical QM. Thus, we get the following system of equations:

$$\begin{aligned} \left(\frac{\partial}{\partial t} + \frac{\gamma_w}{2} + v_g \frac{\partial}{\partial z} \right) a_p(z, t) = \\ \sum_{m=1}^M \sum_{j=1}^{N_m} \Omega_{0,m}(\mathbf{r}_\perp^j) v_m^j(t) \delta(z - z_j), \end{aligned} \quad (7)$$

$$\frac{\partial u_m^j(t)}{\partial t} = -\frac{\gamma}{2} u_m^j(t) - \Delta_j v_m^j(t), \quad (8)$$

$$\begin{aligned} \frac{\partial v_m^j(t)}{\partial t} = & -\frac{\gamma}{2} v_m^j(t) + \Delta_j u_m^j(t) + \\ & \Omega_{0,m}(\mathbf{r}_\perp^j) a_p(z_j, t) w_{3,m}^j(t), \end{aligned} \quad (9)$$

$$\frac{\partial w_{3,m}^j(t)}{\partial t} = -\Omega_{0,m}(\mathbf{r}_\perp^j) a_p(z_j, t) v_m^j, \quad (10)$$

where $E_0 f(\mathbf{r}_\perp) a_p(z, t)$ is an amplitude of p -th light pulse at the point \mathbf{r}^j , $v_m^j(t) = \langle (\sigma_{-,m}^j(t) - \sigma_{+,m}^j(t)) \rangle$, $u_m^j(t) =$

$\langle (\sigma_{-,m}^j(t) + \sigma_{+,m}^j(t)) \rangle$, $w_m^j(t) = \langle \sigma_{3,m}^j(t) \rangle$ are the components of Bloch vector of j_m atom.

B. Pulse area approach

Here, we derive a pulse area approach to describe the general properties of coherent interaction of light pulse with two-level medium in an optical waveguide. We assume that pulse duration of the light pulses (δt_f) is significantly shorter than the phase relaxation time ($T_2 = (\gamma/2)^{-1}$) of the atomic transition ($\gamma \delta t_f \ll 1$). Integrating (7) by time along the envelope of the light pulse from its beginning to the end and using (8)-(10) we get:

$$\begin{aligned} \left(\frac{\partial}{\partial z} + \frac{\gamma_w}{2} \right) \theta_p(z) = \\ \sum_{m=1}^M \sum_{j=1}^{N_m} \frac{\Omega_{0,m}(\mathbf{r}_\perp^j)}{v_g} \int_{t_o}^{t \gg \delta t_f} dt v_m^j(t) \delta(z - z_j) = \\ \frac{2\pi}{v_g} \sum_{m=1}^M \sum_{j=1}^{N_m} \frac{\frac{1}{2}\gamma \Omega_{0,m}^2(\mathbf{r}_\perp^j)}{\pi(\frac{1}{4}\gamma^2 + \Delta_j^2)} \\ \int_{t_o}^{t \gg \delta t_f} dt' w_m^j(t') \alpha_p(z_m^j, t') \delta(z - z_j), \end{aligned} \quad (11)$$

where $\theta_p(z) = \int_{t_o}^{t \gg \delta t_f} dt a_p(z, t)$ is an envelope area.

Then, we transfer from summation of an arbitrary function $F(\mathbf{r}_\perp^j, \Delta_m^j, t)$ to integration assuming a homogeneous distribution of atoms in the waveguide space:

$$\begin{aligned} \sum_{j=1}^{N_m} F(\mathbf{r}_\perp^j, \Delta_m^j, t) \delta(z - z_j) = \\ \rho_m \int d\Delta G\left(\frac{\Delta}{\Delta_{in}}\right) \int_S d\mathbf{r}_\perp F(\mathbf{r}_\perp, \Delta, t), \end{aligned} \quad (12)$$

where $\rho_m = \frac{N_m}{LS}$, N_m are an density and number of m -th group of atoms, L and S - length and cross-section of the waveguide. By taking into account $\Omega_{0,m}(\mathbf{r}_\perp^j) \int_{t_o}^{t \gg \delta t_f} dt' w_m^j(t') \alpha_p(z_m^j, t') = v_m^j(t) - v_m^j(t_0)$, narrow homogeneous linewidth $\frac{\gamma}{\pi(\gamma^2 + \Delta^2)} \cong \delta(\Delta)$ and initial condition $v_m^j(t_0) = 0$, $w_m^j(t_0) = w_0 = -1$, we get for the envelope area $\theta_p(z)$:

$$\frac{\partial}{\partial z} \theta_p(z) = -\frac{\gamma_w}{2} \theta_p(z) - \Phi(\theta_p), \quad (13)$$

$$\Phi(\theta_p) = \sum_{m=1}^M \frac{\beta_m}{2} \int_S d\mathbf{r}_\perp \Omega_{0,m}(\mathbf{r}_\perp) \sin(\Theta_{m,p}(\mathbf{r}_\perp, z)), \quad (14)$$

where the atomic function $\Phi(\theta_p)$ describes the contribution of the total polarization in the fiber cross-section, $\beta_m = \frac{2\pi G(0)\rho_m}{v_g}$, $\Theta_{m,p}(\mathbf{r}_\perp, z) = \Omega_{0,m}(\mathbf{r}_\perp) \theta_p(z)$,

$\Omega_{0,m}(\mathbf{r}_\perp) = \Omega_m f(\mathbf{r}_\perp)$, $\Omega_m = E_0 \langle \mathbf{d}_m \cdot \mathbf{e} \rangle / \hbar$ - Rabi frequency for m -th atoms, for large δ_{in} we can use $G(\frac{\Delta}{\delta_{in}}) = \frac{\delta_{in}}{\pi(\delta_{in}^2 + \Delta^2)}$.

C. Transverse spatial modes

The solution of the (13) strongly depends on the spatial properties of the light modes. Assuming in the simplest case the amplitude of the field is spatially homogeneous in cross-section in (14): $f(\mathbf{r}_\perp) = f_h(\mathbf{r}_\perp) = 1$ characterizing the propagation of a plane wave, we get an atomic function containing various dipole moments (see also [57]):

$$\Phi(\theta_p) = \Phi_h(\theta_p) = \sum_{m=1}^M \frac{S\beta_m \Omega_m}{2} \sin(\Omega_m \theta_p). \quad (15)$$

Using function $\Phi_h(\theta_p)$ in (13) corresponds to the well-known McCall-Hahn pulse area theorem of light pulse propagation in free space for $M = 1$ [5]. In this case, the pulse area of the input pulse Θ asymptotically tends to $\Theta(\kappa_1 z \gg 1) \rightarrow 2n\pi$ for the initial pulse area $(2n-1)\pi < \Theta(0) < (2n+1)\pi$, as shown in the fig. 1 a) (where $\kappa_m = \pi a^2 \Omega_m^2 \beta_m$ is a resonant absorption coefficient of m -th atomic group), which reflects the formation of optical solitons. We pay attention to the transverse light mode with a Gaussian spatial structure of the membrane function:

$$f(\mathbf{r}_\perp) = f_g(\mathbf{r}_\perp/a) = \exp\left\{-\frac{x^2 + y^2}{2a^2}\right\}. \quad (16)$$

Integrating over the cross-section dr_\perp in (14) with $f_g(\mathbf{r}_\perp)$, we get:

$$\left(\frac{\partial}{\partial z} + \frac{\gamma_w}{2}\right)\theta_p = -\Phi_g(\theta_p) = -\sum_{m=1}^M \frac{\kappa_m}{\Omega_m} \frac{\sin^2(\Omega_m \theta_p/2)}{\Omega_m \theta_p/2}. \quad (17)$$

Pulse area theorem (17) with atomic function $\Phi_g(\theta_p)$ (we call it waveguide W-pulse area theorem) shows that $\frac{\partial}{\partial z}\theta_p(z) < 0$ for $2n\pi < \Theta_{m,p} < 2(n+1)\pi$ (where $n = 0, 1, 2, \dots$), $\Theta_{m,p} = \Omega_m \theta_p$ is a pulse area of m -th resonant atoms) and $\frac{\partial}{\partial z}\theta_p(z) = 0$ for $\Theta_{m,p} = 2n\pi$. Thus, if the initial pulse area $\Theta_{m,p}(0)$ is less than 2π , then its pulse area decreases to zero, which differs W-pulse area theorem in waveguide (17) from such theorem in free space [5], where 2π pulse is formed even if $\Theta_{m,p}(0) > \pi$.

In the case of a weak signal pulse ($\Theta_{m,s}(\mathbf{r}_\perp, z) \ll \pi$), we get from (17):

$$\frac{\partial}{\partial z}\theta_s(z) = -\frac{1}{2}(\gamma_w + \sum_{m=1}^M \kappa_m)\theta_s(z), \quad (18)$$

with the Lambert-Beer solution:

$$\theta_s(z) = \theta_s(0)e^{-\alpha z/2}, \quad (19)$$

where $\alpha = \gamma_w + \sum_{m=1}^M \kappa_m$.

Of particular interest is the case when we have only one type of atoms (i.e., $M = 1$ and $\Theta_{m,p}(z) = \Theta_p(z)$) and weak nonresonant losses ($\gamma_w L \ll 1$).

D. The case of a single atomic group (M=1)

In this case, for Gaussian membrane function, we have $\frac{\Omega_1}{\kappa_1}\Phi_g(\theta_p) = \frac{\sin^2(\Theta_p/2)}{\Theta_p/2}$ (where $\Theta_p(z) = \Omega_1 \theta_p(z)$) and the following equation for pulse area $\Theta_p(z)$:

$$\left(\frac{\partial}{\partial z} + \frac{\gamma_w}{2}\right)\Theta_p = -\kappa_1 \frac{\sin^2(\Theta_p/2)}{\Theta_p/2}. \quad (20)$$

Here we have to note that the membrane function of a quasi-linearly polarized mode in a single-mode fiber is most often described by a zero-order Bessel function [58]. Here, we consider two possible cases for filling with atoms of such a fiber. In the first case 1), the atoms are evenly distributed inside the fiber core, and in the second case 2), they are also located in the fiber cladding, filling the entire fiber volume evenly. The membrane functions in these two cases are:

$$f_1(\mathbf{r}_\perp) = \begin{cases} J_0(ur_\perp/a) & r_\perp \leq a \\ 0 & r_\perp > a \end{cases}, \quad (21)$$

$$f_2(\mathbf{r}_\perp) = \begin{cases} J_0(ur_\perp/a), & r_\perp \leq a \\ \frac{J_0(u)}{K_0(w)} K_0(wr_\perp/a) & r_\perp > a \end{cases}, \quad (22)$$

where $J_0(x)$ is Bessel function of the first kind, $K_0(x)$ is modified Bessel function of the second kind, u is the normalized transverse phase constant, w is normalized transverse attenuation constant (propagation constant), a is a fiber core radius.

Using $f_{1,2}(\mathbf{r}_\perp)$, we numerically integrate (14) over the fiber cross-section and find the functions $\frac{\Omega_1}{\kappa_1}\Phi_{1,2}(\theta_p)$ describing the contributions of the total polarization in the equation for the envelope area θ_p for these two cases. The functions $\frac{\Omega_1}{\kappa_1}\Phi_{g,1,2}(\theta_p)$ are presented in fig. 2, where we see that the Gaussian and Bessel modes give very similar results for their atomic functions $\Phi_g(\theta_p)$ and $\Phi_2(\theta_p)$, a slight difference is observed only in the amplitudes and in the region of their minimum values, starting only from the second minimum $\Theta = 4\pi$ where $\Phi_2(\theta_p)$ is not exactly zero. As seen in fig. 2, when atoms are evenly distributed only inside the fiber core, the atomic function $\Phi_1(\theta_p)$ is a slowly decaying alternating oscillatory function. This situation is similar to the case of the McCall and Hahn theorem, where there are regions of values of the pulse

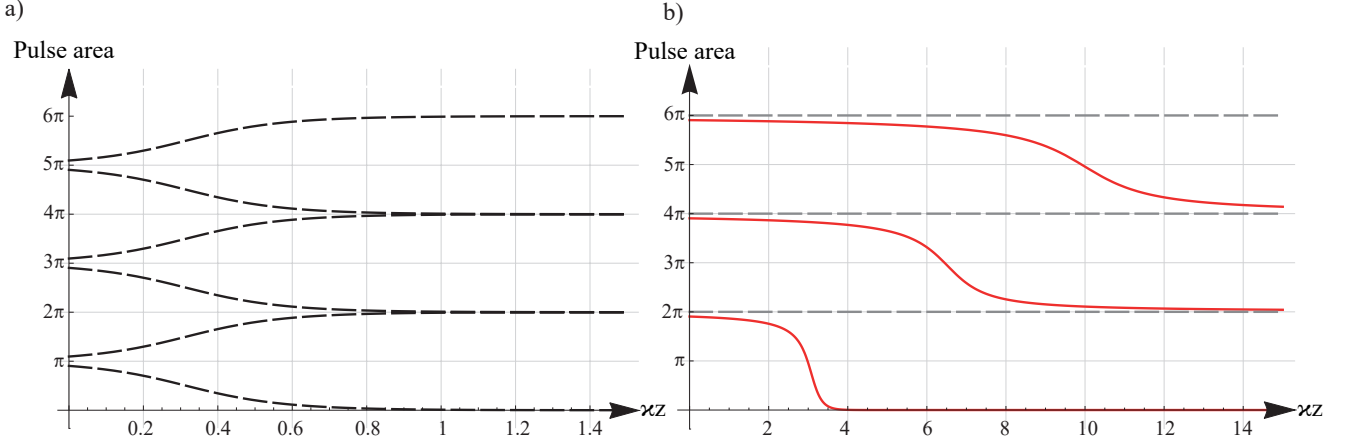


FIG. 1. a) Pulse area $\Theta_p(z)$ of McCall-Hahn area theorem [5] versus optical depth κz for different input pulse areas ($\Theta_p(0) : \pi \pm 0.1, 3\pi \pm 0.1, 5\pi \pm 0.1$); b) pulse area $\Theta_p(z)$ of W-pulse area theorem (23) versus optical depth κz for different input pulse areas ($\Theta_p(0) : 2\pi - 0.2, 4\pi - 0.2, 6\pi - 0.2$); the optical densities of atomic ensembles in the center of the waveguide and in free space are assumed to be equal.

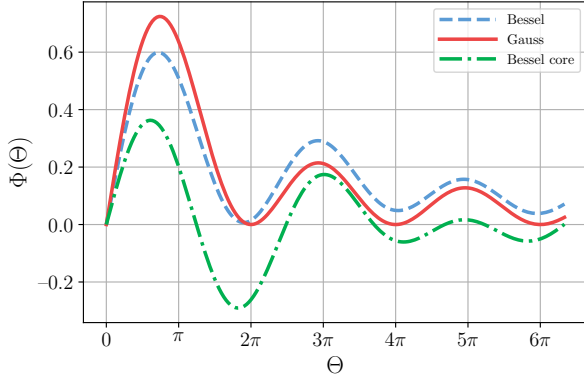


FIG. 2. The atomic functions $\Phi_{g,1,2}(\Theta)$ for Gaussian, Bessel and Bessel core membrane functions $f_{g,1,2}(\mathbf{r}_\perp)$.

area Θ_p with a negative value of the atomic function $\Phi_1(\Theta_p)$. Here there will be an increase in the pulse area for stationary values (to $\Theta_p = 2.5\pi, 4.5\pi$ (see fig. 2)).

Thus, the similarity of functions $\Phi_g(\theta_p)$ and $\Phi_2(\theta_p)$ behavior makes it possible to use an analytical solution of the Gaussian mode to describe both cases at least for $\Theta(0) < 4\pi$. Using the Gaussian mode, we will consider in more detail the evolution of the pulse area in an optically dense medium. For $\gamma_w = 0$, we have an exact analytical solution of (20):

$$T_n(\Theta_p(z)) = T_n(\Theta_p(0)) - \frac{\kappa}{2}z, \quad (23)$$

where

$$T_n(\Theta_p) = \ln(\sin(\frac{\Theta_p}{2})) - (\frac{\Theta_p}{2}) \cot \frac{\Theta_p}{2}. \quad (24)$$

Solution (23), (24) shed light to the main distinctive features of a pulse area behavior in the single mode optical waveguides. The fig. 1 a), b) shows the behavior of the pulse areas for the McCall-Hahn area theorem and the W-pulse area theorem. It is seen in fig. 1 a), b), that in comparison with McCall-Hahn theorem [5], where 2π -pulse can be generated even for initial pulse area $\pi < \Theta_p(0) < 2\pi$, in the waveguide the formation of 2π -pulse is possible only for $\Theta_p(0) > 2\pi n$ where ($n = 1, 2, \dots$). Taking into account that $\frac{\partial}{\partial z} \Theta_p(z) < 0$ for the pulse area $2n\pi < \Theta_p(z) < 2(n+1)\pi$, for $n = 0$ we get in the optically depth medium ($\kappa z \gg 1$): $T_0(\Theta_p(z \gg \kappa^{-1})) \rightarrow \ln(\Theta_p(z)/2)$. In the center of the waveguide mode, the pulse area for atoms with $x = x_0$, $y = y_0$ will evolve asymptotically similar to (19):

$$\Theta_p(z \gg \kappa^{-1}, n = 0) \cong 2 \exp\{T_0(\Theta_p(0)) - \frac{\kappa z}{2}\} \rightarrow 0. \quad (25)$$

Using (24) (for $n = 1, 2, \dots$), we find the asymptotic of $\Theta_p(z, n \neq 0)$ near $2\pi n$:

$$\Theta_p(z \gg \kappa^{-1}, n \neq 0) \cong 2\pi n \left(1 + \frac{1}{\frac{\kappa z}{2} - T_n(\Theta_p(0))}\right) \rightarrow 2\pi n. \quad (26)$$

Thus, the asymptotic behavior of the function $\Theta_p(z \gg \kappa^{-1}, n \neq 0)$ does not have an exponential character and

converges more slowly to its limit compared to the solution $\Theta_p(z \gg \kappa^{-1}, n = 0)$. As it is seen in fig. 1 a), b), the formation of 2π -pulse in waveguide is displaced by almost tenfold greater distance due to the weaker interaction of the waveguide light mode with atoms located closer to the walls of the waveguide, with the same constant of interaction of atoms with the field in the center of the waveguide and in the free space. However, it should be noted that due to spatial confinement and a decrease in the group velocity of light, the constant of its interaction with atoms and, accordingly, the optical density of the medium can even be enhanced significantly in the waveguide. It is also seen in fig. 1 a), b) that in contrast to the solution of McCall-Hahn theorem [5], the formation of the second and subsequent 2π pulses in the waveguide is shifted by a greater distance. At the same time, the solution of (20) is unstable near $\Theta_p = 2\pi n$ in a presence of nonresonant losses ($\gamma_w > 0$) since the losses will continuously decrease the pulse area from $2\pi n$ to $2\pi(n-1)$ with subsequent faster decay to zero due to the stronger interaction with two level atoms. We also see that the solution (23), (24) and fig. 1 b) indicate that the 2π pulse can be quite stable in waveguide for sufficiently weak nonresonant losses.

The presence of several dipole moments and, accordingly, pulse areas $\Theta_{m,p}$ greatly changes the behavior of the pulse area. The formation of 2π pulses (pulses) becomes possible, probably, only if the condition $\Theta_{m,p} = 2n\pi$ is met for each atomic group m . However, this issue requires more detailed research, which is beyond the scope of our analysis.

E. Multipulse excitation and echo signal emission

Here we apply the W-pulse area theorem (13) to photon echo in waveguide and to so-called quantum memory ROSE-protocol [48] when a two-level medium is excited by a weak first signal pulse and then two additional intense control pulses (fig. 3). First control pulse is launched to the medium with time delay τ after signal pulse. Due to the weak signal pulse ($\Theta_{m,s}(\mathbf{r}_\perp, z) \ll \pi$), we have the same equation for the envelope areas of signal θ_s and first exciting control pulse θ_1 ($c = 1$) and can use the solutions of (19), (23), (24). A second control pulse is applied with time delay 2τ after the first control pulse. The propagation of the second controlling intense pulse takes place when atomic inversion is modified by the action of the first controlling pulse [8].

Developing the work [8] on the problem of interaction of atoms with a light pulse in an optical waveguide, we obtain an equation for the envelope area θ_2 ($c = 2$) of the second controlling pulse:

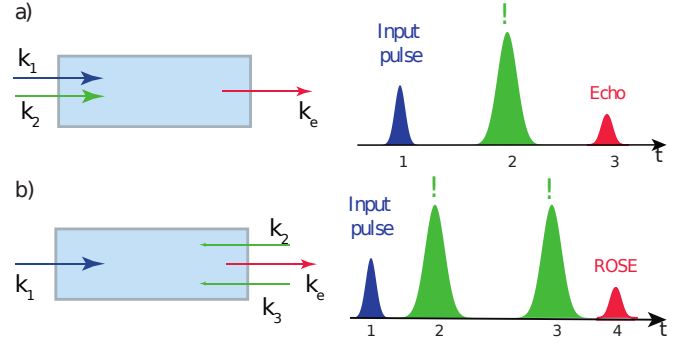


FIG. 3. Spatial schemes and temporal sequences of light pulses in a) the two-pulse (primary) echo, b) the revival of silenced echo (ROSE-protocol).

$$\left(\frac{\partial}{\partial z} + \frac{\gamma_w}{2}\right)\theta_2 = - \sum_{m=1}^M \frac{\beta_m}{2}. \quad (27)$$

$$\int_S d\mathbf{r}_\perp \Omega_{0,m}(\mathbf{r}_\perp) \cos(\Theta_{m,1}(\mathbf{r}_\perp, z)) \sin(\Theta_{m,2}(\mathbf{r}_\perp, z)),$$

where we took into account transverse spatial profile of the control pulse. By using Gaussian membrane function in (27) and performing a calculation similar to (17), we get:

$$\left(\frac{\partial}{\partial z} + \frac{\gamma_w}{2}\right)\theta_2 = - \sum_{m=1}^M \frac{\kappa_m}{\Omega_m} S_m(\theta_2; \theta_1), \quad (28)$$

where

$$S_m(\theta_p; \theta_q) = \frac{1}{2} \sum_{n=1}^2 \frac{\sin^2(\Omega_m(\theta_p + (-1)^n \theta_q)/2)}{\Omega_m(\theta_p + (-1)^n \theta_q)/2}. \quad (29)$$

For the particular case of weak second control field ($\Omega_m \theta_{c2} \ll \pi$), (28) transforms into the linear equation for θ_2 :

$$\left(\frac{\partial}{\partial z} + \frac{\gamma_w}{2}\right)\theta_2(z) = -\frac{1}{2} \sum_{m=1}^M \kappa_m(\Theta_{m,1})\theta_2, \quad (30)$$

where $\kappa_m(\Theta_{m,1}(z))$ is the absorption coefficient of m -th atomic group ($\Theta_{m,1}(z) = \Omega_m \theta_1(z)$):

$$\kappa_m(\Theta_{m,1}(z)) = \kappa_m \left\{ 2 \frac{\sin(\Theta_{m,1}(z))}{\Theta_{m,1}(z)} - \frac{\sin^2(\Theta_{m,1}(z)/2)}{(\Theta_{m,1}(z)/2)^2} \right\}, \quad (31)$$

where $\kappa_m(\Theta_{m,1})$ is negative for $\tan(\Theta_{m,1}/2) > \Theta_{m,1}$ (i.e. $\Theta_{m,1} > 2.3311$), where the second control pulse will be

amplified in the absence of other atomic groups and negligibly weak nonresonant losses $\gamma_w L \ll 1$ ($\varkappa_m(\Theta_{m,1} \rightarrow 0) \rightarrow \varkappa_m$).

The second pulse may experience amplification and attenuation in the medium due to the presence of the first pulse. In this case, the gain of the second pulse is replaced by its weakening to zero ($z \gg 1/\varkappa$). As for the primary (and any other) echo pulse, its pulse area $\Theta_e(z)$ experiences growth reaching a maximum and then decreases to zero. There is a noticeable influence of the parameters of exciting pulses on the amplification of the primary echo at the growth stage.

Next, generalising (27) to the interaction with waveguide mode similar to [9], we get equations for echo pulse area θ_e :

$$\left(\frac{\partial}{\partial z} + \frac{\gamma_w}{2}\right)\theta_e = \sum_{m=1}^M \frac{\beta_m}{2} \int_S d\mathbf{r}_\perp \Omega_{0,m}(\mathbf{r}_\perp) \cdot \left\{ 2\Gamma(\mathbf{r}, \tau, T_M, \Theta_{1,2}) P_m(\mathbf{r}_\perp, z) \cos^2\left(\frac{1}{2}\Theta_{m,e}(\mathbf{r}_\perp, z)\right) + w_m(\mathbf{r}_\perp, z) \sin(\Theta_{m,e}(\mathbf{r}_\perp, z)) \right\}, \quad (32)$$

where $\Gamma(\mathbf{r}, \tau, T_M, \Theta_{1,2})$ is a phase relaxation factor. In the Eqs. (8), (9), (10) we have the simplest relaxation factor $\Gamma(\dots) = e^{-2\tau/T_2}$ for primary echo and $e^{-4\tau/T_2}$ for ROSE-signal. This phase relaxation is slightly corrected in accordance with work [59] by $\Gamma(\dots) = e^{-(2\tau/T_M)^x}$ and $e^{-(4\tau/T_M)^x}$ for primary and ROSE echoes by the power factor x . It should also be noted that other interactions, including those depending on the degree of excitation of atoms, including, for example, the effect of instantaneous spectral diffusion [60, 61]. A more precise elucidation of the nature of phase relaxation and the degree of participation of various interactions in them requires special consideration and experimental research.

F. Two-pulse (primary) echo in optically dense waveguide

Under the studied conditions of atomic excitation, in (32) we have the components of absorbing inversion and phasing coherence for the primary echo [9, 50], generated at moment $t = 2\tau$ (see Fig. 3 a)):

$$\begin{aligned} w_m(\mathbf{r}_\perp, z) &= w_m^{pe}(\mathbf{r}_\perp, z) = -\cos(\Theta_{m,1}(\mathbf{r}_\perp, z)), \\ P_m(\mathbf{r}_\perp, z) &= P_m^{pe}(\mathbf{r}_\perp, z) = \\ &\sin \Theta_{m,s}(\mathbf{r}_\perp, z) \sin^2\left(\frac{1}{2}\Theta_{m,1}(\mathbf{r}_\perp, z)\right). \end{aligned} \quad (33)$$

Here we study the pulse areas of two co-propagating exciting laser pulses, a two-pulse (primary) echo signal and the pulse area of all echo signals under the assumption of weak phase relaxation ($\Gamma(\mathbf{r}, \tau, T_M, \Theta_{1,2}) = 1$). Using the equation for the pulse area of the echo signal (32)

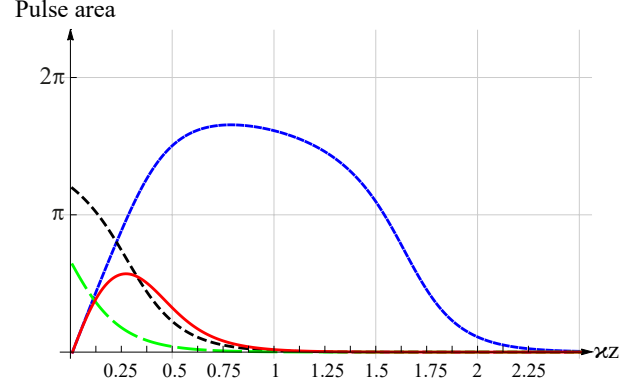


FIG. 4. $\Theta_1(0) + \Theta_2(0) < 2\pi$: pulse area of two exciting pulses (first pulse - green dashed line: $\Theta_1(0) < \pi$, second pulse - black short dashed line: $\pi < \Theta_2(0) < 2\pi$), primary echo (red solid line) and pulse area of all echo pulses (blue dotted line) in single mode waveguide.

and equation (33) for the atomic inversion and the phasing coherence of the two-pulse echo, we will integrate the atomic response along the transverse plane of the waveguide in the same way as calculations (17), resulting in the equation:

$$\left(\frac{\partial}{\partial z} + \frac{\gamma_w}{2}\right)\theta_e = \sum_{m=1}^M \frac{\varkappa_m}{\Omega_m} \left\{ \frac{\Gamma(\tau, T_M, \dots)}{2} I_{s,m}(\theta_s, \theta_1, \theta_2, \theta_e) - S_m(\theta_e; \theta_1; \theta_2) \right\}, \quad (34)$$

where

$$\begin{aligned} I_{s,m}(\theta_s, \theta_1, \theta_2, \theta_e) &= \frac{\sin^2(\Omega_m \theta_s / 2)}{\Omega_m \theta_s / 2} + S_m(\theta_1; \theta_e) \\ &\quad - S_m(\theta_1; \theta_2) - S_m(\theta_1; \theta_2; \theta_e), \end{aligned} \quad (35)$$

$$S_m(\theta_p; \theta_q; \theta_r) =$$

$$\frac{1}{4} \sum_{n=1}^2 \sum_{l=1}^2 \frac{\sin^2(\Omega_m(\theta_p + (-1)^n \theta_q + (-1)^l \theta_r)/2)}{\Omega_m(\theta_p + (-1)^n \theta_q + (-1)^l \theta_r)/2}. \quad (36)$$

The solution of the equations (20), (28), (34) for the pulse areas of the input exciting pulses $\Theta_1(z)$, $\Theta_2(z)$, the primary echo $\Theta_e(z)$ and the total pulse area of all echo signals $\Theta_{\Sigma,e}$ are shown in the figures for the case of one type of atomic dipole moments ($m = 1$). The pulse area of all echo signals $\Theta_{\Sigma,e}$ is defined as the difference between the total pulse area $\Theta_{\Sigma}(z)$ and the pulse areas of two exciting pulses $\Theta_1(z)$, $\Theta_2(z)$ similarly [8], where the evolution of total pulse area $\Theta_{\Sigma}(z)$ is described by (20) with initial pulse area $\Theta_{\Sigma}(0) = \Theta_1(0) + \Theta_2(0)$.

Fig. 4 shows that if the initial total area of the input first two exciting pulses $\Theta_1(0) + \Theta_2(0)$ is less than 2π , then the pulse area of all echo signals $\Theta_{\Sigma,e}(z)$ tends to

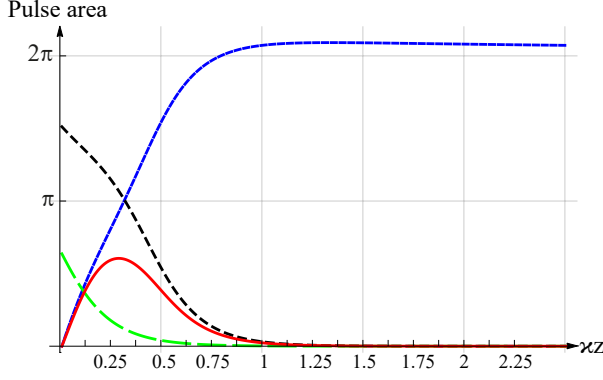


FIG. 5. $2\pi < \Theta_1(0) + \Theta_2(0) < 4\pi$: pulse area of two exciting pulses (first pulse - green dashed line: $\Theta_1(0) < \pi$; second pulse - black short dashed line: $\pi < \Theta_2(0) < 2\pi$), primary echo (red solid line) and pulse area of all echo pulses (blue dotted line) in single mode waveguide.

zero in the depth of the medium $z \gg 1/\kappa$. Whereas if the initial pulse area $\Theta_{\Sigma,e}(0) > 2\pi$, then the pulse area of all echo signals $\Theta_{\Sigma,e}(z \gg 1/\kappa)$ tends to 2π as it is seen in fig. 5. This does not coincide with what is the case for the McCall-Hahn area theorem, where the threshold of the total area is π for 2π pulse formation (see fig. 1a)). As seen in figs. 4, 5 that in both cases, the primary echo amplitude increases with the optical density reaching its maximum, however, its pulse area does not reach up to 2π , therefore, further in the depth of the medium, the primary echo decreases to zero.

Below, we apply the developed theory to the implementation of the photon echo in the so-called ROSE protocol [48, 49], which is the closest to the formation of the primary echo. The considered spatial scheme and temporal sequences of light pulses in ROSE-protocol are shown in fig. 3 b).

III. ROSE PROTOCOL IN A LASER-WRITTEN WAVEGUIDE CRYSTAL

In this protocol, two control laser pulses are used for retrieval of input first weak signal pulse where we have the following atomic inversion $w_m(\mathbf{r}_\perp, z) = w_m^{re}(\mathbf{r}_\perp, z)$ and phasing coherence $P_m(\mathbf{r}_\perp, z) = P_m^{re}(\mathbf{r}_\perp, z)$ [53]:

$$\begin{aligned} w_m^{re}(\mathbf{r}_\perp, z) &= -\cos(\Theta_{m,1}(\mathbf{r}_\perp, z)) \cos(\Theta_{m,2}(\mathbf{r}_\perp, z)), \\ P_m^{re}(\mathbf{r}_\perp, z) &= \sin \Theta_{m,s}(\mathbf{r}_\perp, z) \sin^2\left(\frac{1}{2}\Theta_{m,1}(\mathbf{r}_\perp, z)\right) \cdot \\ &\quad \sin^2\left(\frac{1}{2}\Theta_{m,2}(\mathbf{r}_\perp, z)\right), \end{aligned} \quad (37)$$

where we took into account that the effective pulse area depends on the location of the atom. For the typical quantum memory case, we have weak signal pulse for

which

$$\sin \Theta_{m,s}(\mathbf{r}_\perp, z) \cong \Theta_{m,s}(\mathbf{r}_\perp, z) = \Omega_{0,m}(\mathbf{r}_\perp) \theta_s(0) e^{-\alpha z/2}, \quad (38)$$

is a pulse area of the input signal pulse for the m -th atomic group; the pulse areas of two controlled laser pulses $\Theta_{m,p}(\mathbf{r}_\perp, z) = \Omega_{0,m}(\mathbf{r}_\perp) \theta_p(z)$ ($p=1,2$) should be close to π to achieve high efficiency of the ROSE protocol. We consider the counter-propagating geometry when both control pulses propagate in the opposite direction so " $\frac{\partial}{\partial z}$ " should be replaced by " $-\frac{\partial}{\partial z}$ " in (17), (28)). Control pulses propagating in the opposite direction relative to the direction of propagation of the signal pulse do not cause large optical noise in the echo signal.

We note that $\theta_s, \theta_1, \theta_2$ in (32), (33), (37) can be found according to the Eqs. (17) and (28) for the forward and backward propagation of the control pulses. Similar to discussion of Eqs.(30), (31), we find that the absorption coefficients $\kappa_m(\Theta_1(z); \Theta_2(z))$ in (A6) can be positive or negative, thereby leading to absorption or amplification of echo signal. The last case does not concern QM regime, leading to quantum noise in the echo signal. The solution to this problem in the implementation of quantum memory on a photon echo in optically dense medium was proposed in the work [37], where echo pulse propagates in backward direction to the signal pulse propagation. This (CRIB) protocol serves as the basis for the development of various quantum memory protocols, which differ in the way of control and implementation of inhomogeneous broadening [23, 26]. Generation of the echo signal in the backward direction can provide unity efficiency not only in the photon echo QM protocol [37, 38], but it was also generalized to other protocols [62]. Phase matching condition in CRIB of this protocol is possible for the appropriate wave vectors of the control light pulses [63] and can be extended to more general schemes of reversible interaction dynamics of light pulses with atomic ensembles [64], which makes it possible to effectively change the spectral and time parameters of the echo signal. It is worth noting that practically all photon echo QM protocols can be implemented in a three-level media, where new opportunities appear for quantum processing with signal fields [65] and for developing new methods for generating quantum states of light [66, 67]. For generality, in Appendix A, we give equations for the pulse area of the ROSE echo signal in the waveguide of an optically dense medium for arbitrary intensities of the signal and control fields.

In our experiment, control pulses have phase and amplitude modulation [53], which provides a more uniform spectral and spatial excitation of atoms in the central part of the waveguide cross-section, allowing a significant increase in the efficiency of the echo signal emission (see below).

A. Experimental issues

We implemented ROSE-protocol in the waveguide of crystal $\text{Tm}^{3+}:\text{Y}_3\text{Al}_5\text{O}_{12}$ with doping 0.01 at.% and dimensions $2 \times 9 \times 19.5$ mm. Simplified experimental setup after single mode fibers is shown in Fig. 6 a). Laser light from a single mode fiber is coupled into a single waveguide by objective (Edmund Optics ELWD 10x 59877) by one side and with aspheric lens (Thorlabs A280TM-B) installed into cryostat from another side of the crystal. Light is detected by avalanche photodetector (APD, Thorlabs APD120A/M) connected to oscilloscope (Tektronix DPO7104C) or single photon counting module (SPCM, Excelitas SPCM-AQRH). The crystal is glued by silver paste to cold finger and placed in a closed-cycle cryostat (Montana Instruments Corp.) with temperature 3.2 ± 0.1 K. Crystallographic axes of the crystal are oriented with respect to crystal edges as it is shown in the inset of Fig. 6 a), where $\alpha_E = 11.3^\circ$, $\beta_E = 4.3^\circ$ and $\gamma_E = 0^\circ$ are conventional Euler rotation angles.

The type-III depressed cladding single-mode waveguides were produced by femtosecond laser writing technique in the crystal $\text{Tm}^{3+}:\text{Y}_3\text{Al}_5\text{O}_{12}$ [68]. Each waveguide is composed of 18 elliptical tracks with axes of 2 and $8 \mu\text{m}$ around a circle with diameter of $18 \mu\text{m}$, propagation losses for vertical polarization (parallel to 2 mm edge of the crystal) - 0.66 dB/cm, for horizontal polarization (parallel to 9 mm edge) - 1.13 dB/cm. Twenty one type-III single-mode waveguides were written in the crystal along Z axis. As it follows from our theoretical estimates, the produced waveguide has a Gaussian mode (i.e., the membrane function $f_g(\mathbf{r}_\perp/a)$ in (16)) with half width half maximum of $\sim 5.5 \mu\text{m}$ for both axis (see Fig. 6 b)).

As a radiation source, we used a continuous-wave Titan-Sapphire laser (Tekhnoscan TIS-SF-777). The laser was tuned to $^3\text{H}_6(0) \rightarrow ^3\text{H}_4(0)$ optical transition of Tm^{3+} ($\lambda \approx 793.365$ nm). Two acousto-optical modulators (AOMs) are used to sample microsecond scale pulses for performing two-pulse echo measurements and ROSE protocol. The outputs of AOMs are spatially filtered by single mode fibers and sent parallel to the long edge of the crystal (19.5 mm) in counter-propagating geometry. Here we added the signal beam path where the input pulse propagated as shown in Fig.6a). Both beams were circular-polarized. In the $\text{Y}_3\text{Al}_5\text{O}_{12}$ crystal, Tm^{3+} ions substitute yttrium ions in six ($M = 6$) crystallographically equivalent but orientationally inequivalent sites. In the case of circular polarization, the light beams will interact with all these sites. The Rabi frequency of optical transition $\Omega_m = E_0 \langle \mathbf{d}_m \cdot \mathbf{e} \rangle / \hbar$ is larger for the third and fourth site. In order to get the pulse area of the control pulses to be close to π for the atoms in wider spectral range, we use phase-modulated control laser pulses. The theoretical modeling of the control pulse Rabi frequencies and phase modulation is given by the relations (see also Appendix B):

$$\Omega_m(\tau, \mathbf{r}_\perp) = \Omega_{m,1}(\tau - t_1, \mathbf{r}_\perp) + \Omega_{m,2}(\tau - t_2, \mathbf{r}_\perp), \quad (39)$$

where

$$\Omega_{m,p}(\tau - t_1, \mathbf{r}_\perp) = \dot{A}_{m,p}(\tau - t_p, \mathbf{r}_\perp) e^{-iB_p(\tau - t_p)}, \quad (40)$$

$$\dot{A}_{m,p}(t, \mathbf{r}_\perp) = \frac{\alpha_{m,p}(\mathbf{r}_\perp)}{\pi \delta t_p} \frac{e^{-i\varphi_p}}{\cosh(t/\delta t_p)}, \quad (41)$$

$$\dot{B}_p(t) = \Delta + \frac{\beta_p}{\pi \delta t_p} \tanh(t/\delta t_p). \quad (42)$$

where $\tau = t + z/v_g$, $\alpha_{m,p}(\mathbf{r}_\perp) = \alpha_{0,m,p} f_g(\mathbf{r}_\perp/a)$.

We take into account that the parameters of the control pulses change negligibly weakly in an optically thin medium, so that we can approximate the frequency of the Rabi control fields: $\Omega_{m,c}(\mathbf{r}, t) = \Omega_{0,m}(\mathbf{r}_\perp) a_c(t + z/c)$ (where $c = 1, 2$, $a_c(t + z/v_g) = \langle \hat{a}_c(z, t) \rangle$ is a classical value). The parameters β_p and δt_p responsible for the frequency sweep range and the pulse duration, respectively, were chosen in the range $\beta_p/\pi = 1 \div 7$ and $(2\pi\delta t_p)^{-1} = 140 \div 400$ kHz. The curve with the input pulse was measured by APD/SPAD1, the transmitted part of input pulse and ROSE signal by APD/SPAD2 in Fig.6.

Fig. 7 shows the experimental data of the optical storage of the weak input light pulse obtained in the ROSE protocol in the waveguide. The input signal light pulse (black curve in Fig.7 a)) was launched at $t=0$ and had a Gaussian temporal shape with a $1 \mu\text{s}$ duration (FWHM). The red curve shows the transmitted part of the input pulse. The rephasing pulses are shown at $t = 7.5 \mu\text{s}$ and $t = 22.5 \mu\text{s}$ measured by a detector in the reference channel of rephasing beam. The recovery efficiency of input pulse of 0.5% was achieved for a storage time of $30 \mu\text{s}$. It should be noted that for the used geometry of propagation of the signal and rephasing pulses, as well as the absorption value $\alpha L = 0.12$ and the coherence time of the optical transition $T_M = 63 \mu\text{s}$ ($x = 1.82$), the maximum efficiency of the ROSE-echo is limited by $\eta_{max} = (\alpha L)^2 \cdot e^{-\alpha L} \cdot e^{-2(4\tau/T_M)^x}$ (where 4τ is the storage time), bearing in mind the presence of two ideal control π light pulses. According to this estimation, the maximum achievable efficiency in our optically thin crystal is $\eta_{max} = 0.76\%$. Below we analyze the experimental data obtained for the ROSE protocol in a waveguide using (32), (37), (38) taking into account the experimental parameters of the medium, signal pulses and modeling the parameters of the control pulses by Eqs.(39)-(42).

B. Theoretical discussion of experimental results

In our experiment, the inhomogeneous broadening of the resonant optical transition and the spectra of the control pulses were wider than the spectrum of the signal pulse, so that the temporal shape of the echo signal

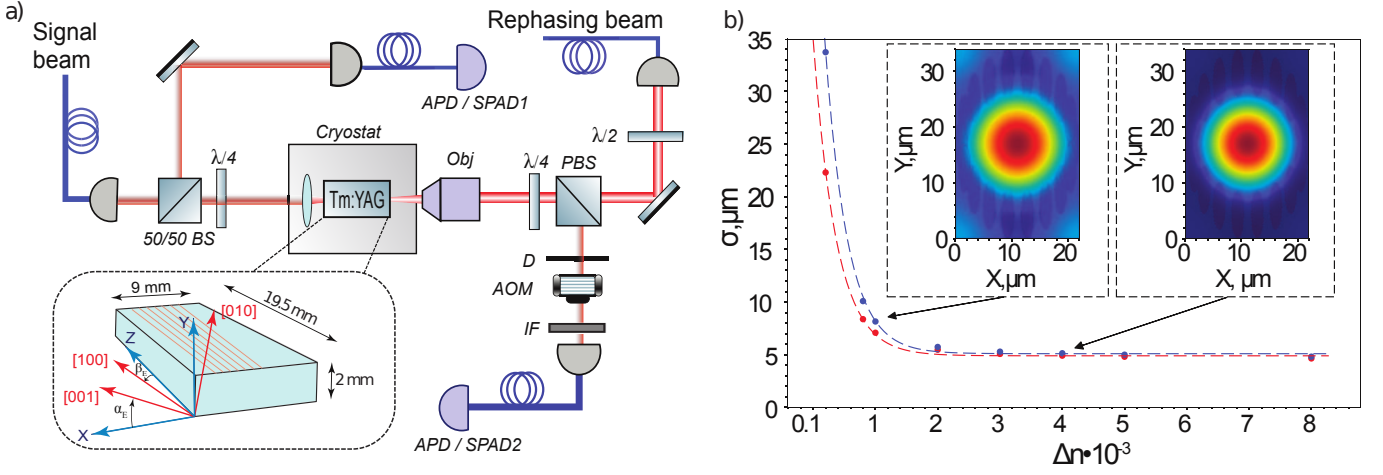


FIG. 6. a). Simplified experimental scheme, where IF is an interference filter, Obj is an objective, also there is one more objective installed inside the cryostat on the left side of the crystal, D is a diaphragm, AOM is an acousto-optic modulator, APD is an avalanche photodiode, SPAD is a single photon avalanche photodiode, $\alpha_E = 11.3^\circ$, $\beta_E = 4.3^\circ$ are conventional Euler rotation angles. Also, we should put SM and MM fiber in the figure. b) The width of the spatial mode Gaussian profile (sigma) in the waveguide in dependence of the refractive index contrast (Δn) between the cladding and the core.

reproduced the temporal shape of the signal pulse, as can be seen in the fig. 7 a), which corresponds to the conditions for the efficient implementation of the photon echo quantum memory [69]. This also allows using Eqs. (32), (33), (37) of the pulse area approach to describe the basic patterns of behavior of the ROSE protocol. Using the analytical solution of the work [70], for excitation of two-level atom \mathcal{P}_{11} by chirped pulse (40)-(42) we get excitation probability of atoms after first (B15) chirped pulse (40), (41), (42) (see Appendix B):

$$\sin^2\left(\frac{1}{2}\tilde{\Theta}_{m,p}(\mathbf{r}_\perp)\right) = \sin^2\left(\frac{1}{2}\Phi_{m,p}(\mathbf{r}_\perp)\right) + \cos^2\left(\frac{1}{2}\Phi_{m,p}(\mathbf{r}_\perp)\right) \tanh^2\left(\frac{\beta}{2}\right), \quad (43)$$

where $\tilde{\Theta}_{m,p}(\mathbf{r}_\perp)$ is an effective pulse area of chirped pulse for resonant atoms ($\Delta = 0$), $p = 1, 2$ (see Appendix B). $\Phi_{m,p}(\mathbf{r}_\perp) = (\alpha_{m,p}^2(\mathbf{r}_\perp) - \beta^2)^{\frac{1}{2}}$, we assume $\beta_p = \beta$.

Taking into account a negligible change in the parameters of the control laser pulses in the optically thin medium, the (32) and weak pulse area of input signal pulse we get a linear equation for echo pulse area:

$$\left(\frac{\partial}{\partial z} + \frac{\gamma_w}{2}\right)\theta_e = \sum_{m=1}^M \frac{\beta_m}{2} \int_S d\mathbf{r}_\perp \Omega_{0,m}(\mathbf{r}_\perp) \cdot \{2\Gamma(\mathbf{r}, \tau, T_M, \Theta_{1,2})P_m(\mathbf{r}_\perp, z) + w_m(\mathbf{r}_\perp, z)\Omega_{0,m}(\mathbf{r}_\perp)\theta_e\}, \quad (44)$$

where $P_m(\mathbf{r}_\perp, z)$ and $w_m(\mathbf{r}_\perp, z)$ are given in (37), (38), $\Gamma(\mathbf{r}, \tau, T_M, \Theta) = e^{-(4\tau/T_M)^x} \exp\{-2\frac{\tau}{T_s(\mathbf{r}_\perp, \Theta, \beta)}\}$ characterizes the phase relaxation of resonant atoms located in a cross-section of the waveguide with a coordinate \mathbf{r}_\perp ;

an additional phase relaxation time $T_s(\mathbf{r}_\perp, \Theta, \beta)$ is determined by relaxation processes depending on the location of the atom in the waveguide (pulse area Θ and β determine the degree of excitation of all atomic groups $m = 1, \dots, M$). It is seen in (47), that the observed phase relaxation factor is an averaged value over the waveguide cross-section and will lead to non-exponential temporal decay. These relaxation processes in the waveguide used should be the subject of additional detailed study, taking into account possible interactions between various thulium ions and imperfections of the created waveguide, their influence on the spectral properties of atoms in the cross section of the waveguide. At the same time, we note that the defects that appeared in the waveguide did not have a dramatically strong negative effect on reducing the phase relaxation time [71].

Firstly, we conducted experiments to study the time decay of the ROSE-echo signal at different intensities of control pulses. The results obtained showed that the effective time of phase relaxation of the ROSE-echo signal depends on the intensity of the control pulses, as shown by red dots in fig. 7 b). We fit the dependence of effective relaxation time $T_s(I, \beta)$ (red solid line in this figure), which depends on the intensity (I) of the control pulses at a given phase modulation (β). Here, we see that the intensity of the control pulses reduces the phase relaxation time of the optical coherence by about 1.5 times (from 67 to 42 μ s) for the concentration of Tm^{3+} 0.01 at.%, which is an order of magnitude less than in the well-known experiments [61], where the attenuation of the echo signal is explained by the influence of the spectral diffusion effect observed earlier.

The detail theory of phase relaxation $T_s(\mathbf{r}_\perp, \Theta, \beta)$ based on experimental results goes out the scope of the paper and will be published somewhere else. However,

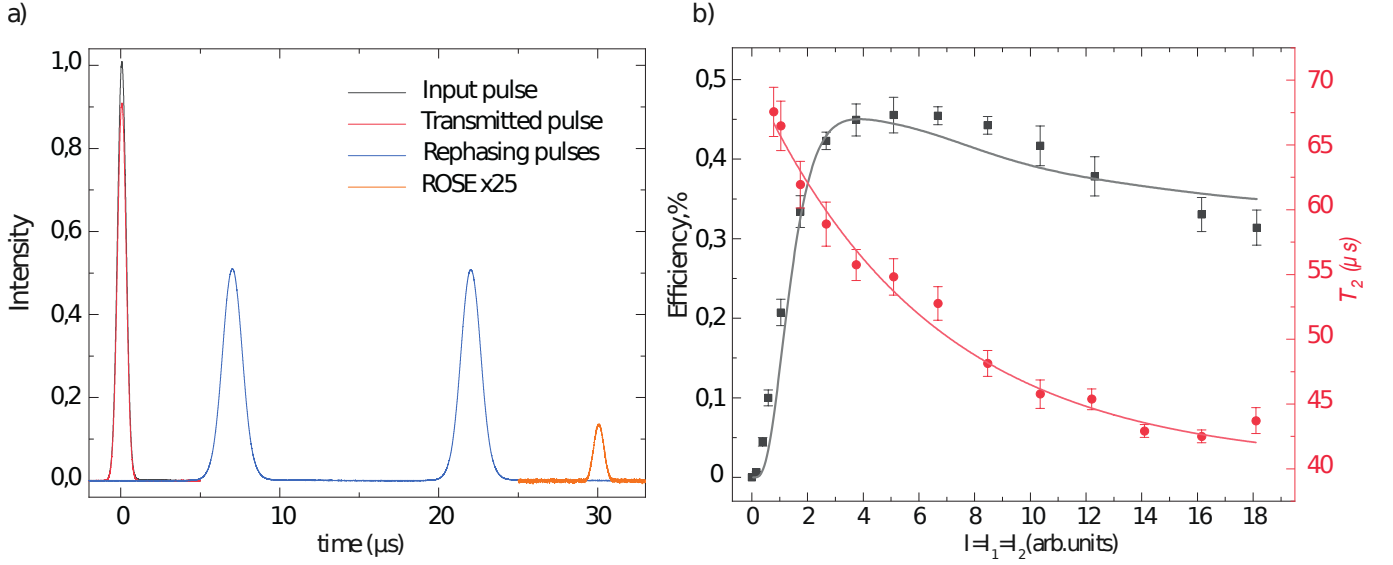


FIG. 7. (a) The signal of the revived of silenced echo magnified by 25 is shown at time 30 μs (green curve) obtained in the waveguide in $\text{Tm}^{3+}:\text{Y}_3\text{Al}_5\text{O}_{12}$ crystal. The rephasing pulses are shown by the blue curve. At $t=0$ μs input pulse and transmitted part are shown by black and red curves, respectively. (b) The retrieval efficiency of input pulse (black squares) and coherence time T_2 of optical transition measured by ROSE sequence (red circles) in a waveguide optical memory versus intensity of rephasing pulses in the case then $I = I_1 = I_2$.

taking into account the experimental data obtained, we will limit ourselves to the effective constant of phase relaxation $1/T_s(I, \beta)$. By assuming the parameters of the two control pulses to be equal $\tilde{\Theta}_{m,2}(\mathbf{r}_\perp, z) = \tilde{\Theta}_{m,1}(\mathbf{r}_\perp, z)$, the solution of (44) is:

$$\theta_e(z, \beta, \tau) = 2 \frac{e^{-(4\tau/T_M)^x} A_w(I, \Theta, \beta, \tau) \theta_s(0)}{(\alpha_w - \alpha) (e^{-\frac{1}{2}\alpha z} - e^{-\frac{1}{2}\alpha_w z})}, \quad (45)$$

where $A_w(I, \Theta, \beta, \tau) = \sum_{m=1}^M A_{0,m}(I, \beta, \tau)$, $\alpha_w = \gamma_w + \sum_{m=1}^M \kappa_{m,w}$ is an absorption coefficient for echo pulse,

$$\kappa_{m,w} = \frac{\beta_m}{2} \int_S d\mathbf{r}_\perp \Omega_{0,m}^2(\mathbf{r}_\perp) \cos^2(\tilde{\Theta}_{m,1}(\mathbf{r}_\perp)), \quad (46)$$

$$A_{0,m}(I, \beta, \tau) = \beta_m \exp\left\{-\frac{2\tau}{T_s(I, \beta)}\right\} \int_S d\mathbf{r}_\perp \Omega_{0,m}^2(\mathbf{r}_\perp) \sin^4\left(\frac{1}{2}\tilde{\Theta}_{m,1}(\mathbf{r}_\perp)\right). \quad (47)$$

In optically thin media ($\alpha L \ll 1, \alpha_w L \ll 1$) from (45) we have at the output of the medium ($z = L$):

$$\theta_e(L, I, \Theta, \beta, \tau) = e^{-(4\tau/T_M)^x} \theta_s(0) A_w(I, \Theta, \beta, \tau) L. \quad (48)$$

The function $A_w(I, \Theta, \tau)$ together with $e^{-(4\tau/T_M)^x}$ describes all the basic properties of the ROSE-echo in the waveguide: the influence of the transverse structure of

the waveguide light modes, intensity and chirping of control pulses, as well as the intensity dependent phase relaxation $\exp\{-\frac{2\tau}{T_s(I, \beta)}\}$. Fig. 7 b) (black dots) shows experimental data on the ROSE echo signal intensity depending on the intensity of two control laser pulses having equal pulse areas. Here, one can see that the echo-signal increases with the intensity of the control pulses and, having reached a maximum, further decreases slightly. Thus, despite the high value of the Rabi frequency ($\Theta > \pi$) of the control laser pulses, no nutations have been observed experimentally. The weakening of the nutations in echo signal is possible due to the inhomogeneity of the intensity of the control pulses [51], which takes place for atoms located in different coordinates of the cross-section of the waveguide. In our case, the suppression of nutations in the echo signal is due to the presence of phase modulation of the control pulses.

The experimental data are satisfactorily described by $|\theta_e(L, I, \Theta, \beta_p/\pi, \tau, \delta t_p)|^2$ (see Eq.(48)) with $\beta_p/\pi = 7$, $\tau = 8.5$, $\delta t_p = 3$, which is shown by solid black curve in Fig. 7 b). The relatively large value of $\beta_p/\pi = 7$ can be explained by the difference in the experimentally realized envelope of the control pulses, namely, the reduced central part of the pulses compared to its fronts. Analyzing the above results, we can conclude that it is the instantaneous spectral diffusion that affects the drop in the efficiency of the suppressed echo signal recovery. There is a slight difference between the experimental data and the theoretical curve of echo attenuation with increasing intensity of control pulses. The difference may be due to a number of reasons, including an approximate description of the dependence of phase relaxation on the intensity of

the control pulses. Note that the characteristic feature of the echo signal intensity growth is proportional to intensity of control pulses $\sim I^2$, but not to $\sim I^4$, which would happen when using spectrally limited controlling laser pulses and, accordingly, is unrecognized indicates the influence of phase modulation of controlling laser pulses.

IV. CONCLUSION

In this work, we derived the pulse area theorem (W-pulse area theorem) for resonant interaction of light pulses with two-level medium in single mode optical waveguide. We found an analytical solution to this theorem for a light mode with a Gaussian intensity profile. Possibility of 2π pulses formation for fundamental Gaussian and Bessel light modes was shown. The specific properties and differences of these 2π pulses are characterized in comparison with formation 2π pulses described by McCall-Hahn area theorem [5]. The prediction of the formation of a 2π pulses in a single-mode fiber raises the question of the spatial-temporal structure of the resulting light pulses, which is the topic of future research.

Next, we developed W-pulse area theorem for studies of photon echo in single mode waveguide and applied it for analysis of two-pulse (primary) photon echo and analysis of photon echo quantum memory protocol based on so called ROSE-echo. For the first time, the ROSE protocol was implemented in an optically thin single-mode waveguide structure in a $\text{Tm}^{3+}:\text{Y}_3\text{Al}_5\text{O}_{12}$ crystal. In the experiment, the recovery efficiency of input pulses was 0.5 % for a storage time of 30 μs . The storage of coherent optical pulses attenuated to the level of one photon in the reconstructed signal of the silent echo for a single signal-to-noise level has been achieved. In these experiments, for the first time, we observed influence of intensity of control laser pulse on the phase relaxation of ROSE echo in crystal with the lowest concentration 0.01 % of Tm^{3+} ions in a $\text{Tm}^{3+}:\text{Y}_3\text{Al}_5\text{O}_{12}$ crystal. It was observed that despite the use of rephasing pulses with amplitude and frequency modulation, with an increase in the intensity, the retrieval efficiency of the input signal decreased.

The theoretical analysis carried out, based on the use of the W-pulse area theorem, allowed us to satisfactorily explain the experimental data obtained. The decrease in the echo signal with an increase in the intensity of the controlling laser pulses is explained by a decrease in the phase relaxation time, which could be explained by the effect of instantaneous spectral diffusion. In this case, we have detected the manifestation of instantaneous spectral diffusion for lowest concentration of thulium ions in this crystal. In order to highly suppress the negative effect of instantaneous spectral diffusion for the implementation of QM on photon echo, one can use the crystals with lower concentration of working atoms, which is possible, for example, for the QM protocols in high-quality optical resonators [47]. It is worth noting, as we have shown here, that not only the presence of pure dephasing and

instantaneous spectral diffusion [61, 72] will limit the efficiency of the ROSE protocol in the waveguide, but also difficulties in achieving an ideal control laser π pulse for the uniform distribution of working atoms in the waveguide cross-section. The creation of waveguides with the working atoms located near the axis of the waveguide is of great interest for subsequent research.

The performed research demonstrates the usefulness of the pulse area approach for studies of the nonlinear interaction, propagation of the stationary (soliton-like) light pulses and description of photon echo for QM protocols in single-mode optical waveguides. The obtained results raise the question of the development and application of this approach to the formation of stable light pulses and photon echo signals in other waveguides.

ACKNOWLEDGMENTS

This research was supported by the Ministry of Science and Higher Education of the Russian Federation (Reg. number NIOKTR 121020400113-1). SPK is supported by the Ministry of Science and Higher Education of the Russian Federation on the basis of the FSAEIH SUSU (NRU) (Agreement No. 075-15-2022-1116).

Appendix A: ROSE-protocol in optically dense waveguide

Here we assume that signal and control fields have the same carrier frequency without phase modulation. Using $w_m^{re}(\mathbf{r}_\perp, z)$ and $P_m^{re}(\mathbf{r}_\perp, z)$ in (32) together with phase relaxation function $\Gamma(\mathbf{r}, \tau, T_M, \Theta_{c1,c2})$ we can perform general analysis of nonlinear pattern in ROSE-pulse area behavior.

In the simplest case of negligible spatial dependence of phase relaxation (i.e., $\Gamma(\mathbf{r}, \tau, T_2, \Theta_{c1,c2}) = \Gamma(\tau, T_2, \dots)$), we can perform analytical integration and subsequent calculation of (32) similar to (28) and to get the following equation for ROSE-echo field envelope:

$$\left(\frac{\partial}{\partial z} + \frac{\gamma_w}{2}\right)\theta_e = \sum_{m=1}^M \frac{\varkappa_m}{\Omega_m} \left\{ \frac{\Gamma(\tau, T_M, \dots)}{4} I_{s,m}(\theta_s, \theta_1, \theta_2, \theta_e) - S_m(\theta_e; \theta_1; \theta_2) \right\}, \quad (\text{A1})$$

where $\theta_{s,1,2,e} = \theta_{s,1,2,e}(z)$ are the functions of z and a source of echo signal:

$$\begin{aligned} I_{s,m}(\theta_s, \theta_{c1}, \theta_{c2}, \theta_e) = & \frac{1}{2} \Omega_m \theta_s(z) + S_m(\theta_s; \theta_e) + S_m(\theta_s; \theta_1; \theta_2) \\ & - S_m(\theta_s; \theta_e; \theta_1) - S_m(\theta_s; \theta_e; \theta_2) + S_m(\theta_s; \theta_e; \theta_1; \theta_2), \end{aligned} \quad (\text{A2})$$

we also taken into account that the pulse area of signal pulse $\Omega_m \theta_s(z) \ll \pi$ and

$$\begin{aligned}
S_m(\theta_1; \theta_2; \theta_3) &= \\
\frac{1}{4} \sum_{n=1}^2 \sum_{m=1}^2 \frac{\sin^2(\Omega_m(\theta_1 + (-1)^n \theta_2 + (-1)^m \theta_3)/2)}{\Omega_m(\theta_1 + (-1)^n \theta_2 + (-1)^m \theta_3)/2}, \\
S_m(\theta_1; \theta_2; \theta_3; \theta_4) &= \frac{1}{8} \sum_{n=1}^2 \sum_{m=1}^2 \sum_{p=1}^2 \\
\frac{\sin^2(\Omega_m(\theta_1 + (-1)^n \theta_2 + (-1)^m \theta_3 + (-1)^p \theta_4)/2)}{\Omega_m(\theta_1 + (-1)^n \theta_2 + (-1)^m \theta_3 + (-1)^p \theta_4)/2}.
\end{aligned} \quad (\text{A3})$$

(A1) is a nonlinear equation on θ_e . It is possible to find its solution in the case weak input signal $\Omega_m \theta_s(z) \ll \pi$ for the medium with limited optical density, where $\Omega_m \theta_e(z) \ll \pi$ will be executed in the waveguide ($0 < z < L$). Neglecting the terms with $(\Omega_m \theta_e)^2 \ll \pi$ in (A1), we get the equation for θ_e in this case:

$$\begin{aligned}
\left(\frac{\partial}{\partial z} + \frac{\gamma_w}{2}\right)\theta_e &= \sum_{m=1}^M \left\{ \frac{\varkappa_m}{4\Omega_m} \Gamma(\tau, T_2, \dots) I_{s,m}(\theta_s, \theta_{c1}, \theta_{c2}) \right. \\
&\quad \left. - \frac{1}{2} \varkappa_m(\theta_{c1}; \theta_{c2}) \theta_e \right\},
\end{aligned} \quad (\text{A4})$$

where $I_{s,m}(\theta_s, \theta_{c1}, \theta_{c2}) \equiv I_{s,m}(\theta_s, \theta_{c1}, \theta_{c2}, 0)$:

$$\begin{aligned}
I_{s,m}(\theta_s, \theta_{c1}, \theta_{c2}) &= \Omega_m \theta_s - S_m(\theta_s; \theta_{c1}) - \\
&\quad S_m(\theta_s; \theta_{c2}) + 2S_m(\theta_s; \theta_{c1}; \theta_{c2}),
\end{aligned} \quad (\text{A5})$$

and absorption coefficient for echo signal due to the interaction with m -th atomic group:

$$\begin{aligned}
\varkappa_m(\theta_{c1}; \theta_{c2}) &= \varkappa_m \sum_{n=1}^2 \left\{ \frac{\sin(\Omega_m(\theta_{c1} + (-1)^n \theta_{c2}))}{\Omega_m(\theta_{c1} + (-1)^n \theta_{c2})} \right. \\
&\quad \left. - \frac{\sin^2(\Omega_m(\theta_{c1} + (-1)^n \theta_{c2})/2)}{2(\Omega_m(\theta_{c1} + (-1)^n \theta_{c2})/2)^2} \right\}.
\end{aligned} \quad (\text{A6})$$

Appendix B: Excitation of atoms by controlling chirped pulses

Here following [70], we consider the excitation of two-level atoms by two chirped control pulses. In the interaction picture, the equations for atomic amplitudes in the ground $C_2(t)$ and exited $C_1(t)$ states are:

$$\begin{pmatrix} \dot{C}_1(t) \\ \dot{C}_2(t) \end{pmatrix} = \frac{i}{2} \begin{pmatrix} 0 & \Omega(t) \\ \Omega^*(t) & 0 \end{pmatrix} \begin{pmatrix} C_1(t) \\ C_2(t) \end{pmatrix}, \quad (\text{B1})$$

with initial state $C_2(t \rightarrow -\infty) = 1$, $C_1(t \rightarrow -\infty) = 0$ where

$$\begin{aligned}
\Omega(t) &= \Omega_1(t - t_1) + \Omega_2(t - t_2) \\
&= (\dot{A}_1(t) e^{-iB_1(t)} + \dot{A}_2(t) e^{-iB_2(t)}) e^{-i\Delta(t-t_0)},
\end{aligned} \quad (\text{B2})$$

$$\dot{A}_p(t) = \frac{\alpha_p}{\pi \tau_p} \frac{e^{-i\varphi_p}}{\cosh[(t - t_p)/\tau_p]}, \quad (\text{B3})$$

$$\dot{B}_p(t) = \frac{\beta_p}{\pi \tau_p} \tanh[(t - t_p)/\tau_p]. \quad (\text{B4})$$

where $p = 1, 2$, $A_p(t)$ - Rabi frequency of the pulses, in particular, we also assume that it can be a function of transverse coordinate \mathbf{r}_\perp : $\alpha_p(\mathbf{r}_\perp) = \alpha_{p,0} f(\mathbf{r}_\perp)$; φ_p - constant phases; $B_p(p)$ describes frequency modulation; Δ - atomic detuning.

By taking into account that these two pulses are not overlapped ($\tau_{1,2} \ll t_1 - t_0, t_2 - t_1$) we can solve the equations one by one. For each pulse the solution (B1) can be written in terms of Hypergeometric functions where it is convenient writing $C_p(t)$ via new variable

$$z_1(t) = \frac{1}{2}(1 + \tanh[(t - t_1)/\tau_1]), \quad (\text{B5})$$

($C_p(t) = \tilde{C}_p(z_1)$) and determining the phase of the first light pulse φ_1 by setting $B_1(t) = \int_{t_0}^t dt' \dot{B}_1(t')$. The atomic amplitudes at the interaction with the first pulse (starting at $t = t_0$) is described by

$$\tilde{C}_1(z_1) = A_1^{(12)} z_1^{1-c_1} \mathcal{F}_1^{(1)}(z_1), \quad (\text{B6})$$

$$\tilde{C}_2(z_1) = C_2(t_0) \mathcal{F}_1^{(2)*}(z_1), \quad (\text{B7})$$

where we introduced an abbreviated notation for hypergeometric functions:

$$\mathcal{F}_p^{(1)}(z_p) = F(a_p + 1 - c_p, b_p + 1 - c_p, 2 - c_p, z_p), \quad (\text{B8})$$

$$\mathcal{F}_p^{(2)*}(z_p) = F^*(a_p, b_p, c_p, z_p) = F(a_p^*, b_p^*, c_p^*, z_p), \quad (\text{B9})$$

bottom index $p = 1, 2$ corresponds to the interaction with 1-st, 2-nd control pulse,

$$A_1^{(12)} = \frac{i\alpha_1 e^{-i\varphi_1}}{2\pi(1 - c_1)} C_2(t_0) \exp\{i(\Delta - \frac{\beta_1}{\pi\tau_1})(t_0 - t_1)\}, \quad (\text{B10})$$

Values a_p, b_p, c_p can be found in [70]:

$$a_p = \frac{1}{2\pi} [(\alpha_p^2 - \beta_p^2)^{\frac{1}{2}} - i\beta_p], \quad (\text{B11})$$

$$b_p = \frac{1}{2\pi} [-(\alpha_p^2 - \beta_p^2)^{\frac{1}{2}} - i\beta_p], \quad (\text{B12})$$

$$c_p = \frac{1}{2} \left[1 + i \frac{\pi \Delta \tau_p - \beta_p}{\pi} \right]. \quad (\text{B13})$$

Interaction with the first pulse ends for $t - t_1 \gg \tau_1$ when $z_1 \rightarrow 1$ and the amplitudes $\tilde{C}_{1,2}(z = 1)$ are set unchanged. Probability to find atom excited after the impact of the first pulse for $|C_2(t_0)| = 1$ in (B7):

$$\mathcal{P}_{11}(t_1) \equiv P_{11}(t \gg t_1 + \tau_1) = |\tilde{C}_1(1)|^2 = \sin^2(\Theta_1/2), \quad (\text{B14})$$

where

$$\frac{\alpha_p^2 |\mathcal{F}_p^{(1)}(1)|^2}{4\pi^2 |1 - c_p|^2} = \sin^2(\Theta_p/2) = \frac{\sin^2(\Phi_p/2) Ch^2(\beta_p/2) + \cos^2(\Phi_p/2) Sh^2(\beta_p/2)}{Ch(\frac{\beta_p + \pi \Delta \tau_p}{2}) Ch(\frac{\beta_p - \pi \Delta \tau_p}{2})}, \quad (\text{B15})$$

where $\Phi_p = (\alpha_p^2 - \beta_p^2)^{\frac{1}{2}}$ ($p=1,2$) and (B14), (B15) are also used to define the nutation angle of two-level atom $\Theta_{p=1} = \Theta_1(\Delta, \beta_1, \Phi_1)$ by first pulse. By using (B15), we can easily calculate $|\mathcal{F}_1^{(2)}(1)|^2$ and the probability of atom to stay on the ground level $P_2(t \gg t_1 + \tau_1) = |C_2(t \gg t_1)|^2 = |\tilde{C}_2(1)|^2 = |\mathcal{F}_1^{(2)}(1)|^2 = 1 - |\tilde{C}_2(1)|^2 = \cos^2(\Theta_1/2)$, so we get

$$C_2(t \gg t_1) = \mathcal{F}_1^{(2)*}(1) = \cos(\Theta_1/2) \exp\{-i\chi_1(\Delta, \alpha_1, \beta_1, \tau_1)\}, \quad (\text{B16})$$

where $\chi_1(\Delta, \alpha_1, \beta_1, \tau_1) = -i \ln\{\mathcal{F}_1^{(2)}(1)/\cos(\Theta_1/2)\}$.

Interaction with the second pulse occurs at t_2 with sufficiently large time delay $t_2 - t_1 \gg \tau_1$. Let's chose a moment in time in the middle between the pulses $t_m = \frac{t_1 + t_2}{2}$. Using (B1) for $t > t_m$ we can describe the interaction with the second pulse similarly to the interaction with the first pulse, moving to new amplitudes $C_{2,0}(t) = C_2(t) \exp\{-\frac{i}{2}\Delta(t_m - t_0)\}$, $C_{1,0}(t) = C_1(t) \exp\{\frac{i}{2}\Delta(t_m - t_0)\}$. Here we get the following system of equations for $C_{1,0}(t)$ and $C_{2,0}(t)$ ($t > t_m$), that takes into account the phase change in the frequency of the second pulse at the time of the beginning of the interaction:

$$\begin{pmatrix} \dot{C}_{1,0}(t) \\ \dot{C}_{2,0}(t) \end{pmatrix} = \frac{i}{2} \begin{pmatrix} 0 & \Omega_2(t - t_m) \\ \Omega_2^*(t - t_m) & 0 \end{pmatrix} \begin{pmatrix} C_{1,0}(t) \\ C_{2,0}(t) \end{pmatrix}, \quad (\text{B17})$$

with initial amplitudes:

$$C_{2,0}(t_m) = \tilde{C}_2(1) \exp\{-\frac{i}{2}\Delta(t_m - t_0)\}, \quad (\text{B18})$$

$$C_{1,0}(t_m) = \tilde{C}_1(1) \exp\{\frac{i}{2}\Delta(t_m - t_0)\}, \quad (\text{B19})$$

where $\Omega_2(t - t_m) = \dot{A}_2(t) \exp\{-i[B_2(t) + \Delta(t - t_m)]\}$ and the constant phase of the second light pulse φ_2 .

Similarly to the interaction with the first pulse, we move to a new time variable scale $z_2 = \frac{1}{2}(1 + \tanh[(t - t_2)/\tau_2])$, and find solutions of $C_{p,0}(t > t_m) = \tilde{C}_{p,0}(z_2)$ with initial conditions $\tilde{C}_{p,0}(0) = C_{p,0}(t_m)$:

$$\tilde{C}_{1,0}(z_2) = C_{1,0}(t_m) \mathcal{F}_2^{(2)}(z_2) + A_2^{(12)} z_2^{1-c_2} \mathcal{F}_2^{(1)}(z_2), \quad (\text{B20})$$

$$\tilde{C}_{2,0}(z_2) = C_{2,0}(t_m) \mathcal{F}_2^{(2*)}(z_2) + A_2^{(21)} z_2^{1-c_2^*} \mathcal{F}_2^{(1*)}(z_2), \quad (\text{B21})$$

where

$$A_2^{(12)} = \frac{i\alpha_2 e^{-i\varphi_2}}{2\pi(1 - c_2)} C_{2,0}(t_m) \exp\{i(\Delta - \frac{\beta_2}{\pi\tau_2})(t_m - t_2)\}, \quad (\text{B22})$$

$$A_2^{(21)} = \frac{i\alpha_2 e^{i\varphi_2}}{2\pi(1 - c_2^*)} C_{1,0}(t_m) \exp\{-i(\Delta - \frac{\beta_2}{\pi\tau_2})(t_m - t_2)\}. \quad (\text{B23})$$

The probability of the atomic excitation $\mathcal{P}_{11}(t_2) \equiv P_{11}(t \gg (t_2 + \tau_2)) = |\tilde{C}_{1,0}(z_2 = 1)|^2$ after interaction with two pulses excitation will be:

$$\mathcal{P}_{11}(t_2) = |\tilde{C}_{1,0}(1)|^2 = |C_{1,0}(t_m) \mathcal{F}_2^{(2)}(1)|^2 + |A_2^{(12)} \mathcal{F}_2^{(1)}(1)|^2 + (\delta\mathcal{P}_{coh}(t_2) + C.C.), \quad (\text{B24})$$

where we have:

$$|C_{1,0}(t_m) \mathcal{F}_2^{(2)}(1)|^2 = \sin^2(\Theta_1/2) \cos^2(\Theta_2/2), \quad (\text{B25})$$

$$|A_2^{(12)} \mathcal{F}_2^{(1)}(1)|^2 = \sin^2(\Theta_2/2) \cos^2(\Theta_1/2), \quad (\text{B26})$$

and interference term:

$$\begin{aligned} \delta\mathcal{P}_{coh}(t_2) &= C_{1,0}(t_m) A_2^{(12)*} \mathcal{F}_2^{(2)}(1) = \\ &= \exp\{i[\delta\varphi + \tilde{\varphi}_{2,1} + \Delta(t_2 - t_1)]\} \cdot \\ &\frac{\alpha_1 \alpha_2 \mathcal{F}_1^{(1)}(1) \mathcal{F}_2^{(1*)}(1)}{4\pi^2 (1 - c_1)(1 - c_2^*)} \mathcal{F}_1^{(2)}(1) \mathcal{F}_2^{(2)}(1). \end{aligned} \quad (\text{B27})$$

where $\delta\varphi$ - a random phase occurring at an atom during the time interval $t_2 - t_1$ of free evolution, $\tilde{\varphi}_{2,1} = \tilde{\varphi}_2 - \tilde{\varphi}_1$, $\tilde{\varphi}_p$ - constant phases of p-th control pulses are defined by setting $B_{1,2}(t) = \int_{t_0, t_m}^t dt' \dot{B}_2(t')$ as follows: $\tilde{\varphi}_1 = \varphi_1 + \frac{\beta_1}{\pi\tau_1}(t_0 - t_1)$, $\tilde{\varphi}_2 = \varphi_2 + \frac{\beta_2}{\pi\tau_2}(t_m - t_2)$. In (B27) we also used: $C_{1,0}(t_m) = \tilde{C}_1(1) \exp\{\frac{i}{4}\Delta(t_m - t_0)\}$, $\tilde{C}_1(1) = A_1^{(12)} \mathcal{F}_1^{(1)}(1)$, and $C_{2,0}(t_m) = \tilde{C}_2(1) \exp\{-\frac{i}{4}\Delta(t_m - t_0)\}$, $\tilde{C}_2(1) = \mathcal{F}_1^{(2*)}(1)$.

In particular case of identical control pulses ($\alpha_1 = \alpha_2, \beta_1 = \beta_2, \tau_1 = \tau_2$ and $\Theta_1 = \Theta_2$, respectively), we get:

$$\begin{aligned} \mathcal{P}_{11}(t_2; \Theta_2 = \Theta_1) &= \\ \frac{1}{2} \sin^2 \Theta_1 \{1 + \cos[\delta\varphi + 2\chi_1 + \Delta(t_2 - t_1)]\}. \end{aligned} \quad (\text{B28})$$

where χ_1 is given in (B16).

Below, we have taken into account Gaussian membrane function in Rabi frequency of the control fields: $\alpha_p(\mathbf{r}_\perp) = \alpha_{p,0} f_g(\mathbf{r}_\perp)$.

- [1] L. Allen and J. Eberly, *Optical Resonance and Two-level Atoms*, Dover books on physics and chemistry (Dover, 1975) p. 256.
- [2] M. O. Scully and M. S. Zubairy, *Quantum Optics* (Cambridge University Press, 1997).
- [3] R. W. Boyd, *Nonlinear optics*, 2nd ed. (ACADEMIC PRESS, 2003).
- [4] N. Sangouard, C. Simon, H. de Riedmatten, and N. Gisin, Quantum repeaters based on atomic ensembles and linear optics, *Rev. Mod. Phys.* **83**, 33 (2011).
- [5] S. L. McCall and E. L. Hahn, Self-induced transparency, *Phys. Rev.* **183**, 457 (1969).
- [6] R. Gutiérrez-Cuevas and J. H. Eberly, Vector-soliton storage and three-pulse-area theorem, *Phys. Rev. A* **94**, 013820 (2016).
- [7] C. Greiner, T. Wang, T. Loftus, and T. W. Mossberg, Instability and pulse area quantization in accelerated superradiant atom-cavity systems, *Phys. Rev. Lett.* **87**, 253602 (2001).
- [8] E. L. Hahn, N. S. Shiren, and S. L. McCall, Application of the area theorem to phonon echoes, *Physics Letters A* **37**, 265 (1971).
- [9] S. A. Moiseev, M. Sabooni, and R. V. Urmanceev, Photon echoes in optically dense media, *Phys. Rev. Research* **2**, 012026 (2020).
- [10] S. A. Moiseev and R. V. Urmanceev, Photon/spin echo in a fabry-perot cavity, *Opt. Lett.* **47**, 3812 (2022).
- [11] J.-H. Kim, S. Aghaeimeibodi, J. Carolan, D. Englund, and E. Waks, Hybrid integration methods for on-chip quantum photonics, *Optica* **7**, 291 (2020).
- [12] Y. Hibino, Silica-based planar lightwave circuits and their applications, *MRS Bull.* **28**, 365 (2003).
- [13] A. Rodenas and A. K. Kar, High-contrast step-index waveguides in borate nonlinear laser crystals by 3D laser writing, *Opt. Express* **19**, 17820 (2011).
- [14] A. G. Okhrimchuk, A. V. Shestakov, I. Khrushchev, and J. Mitchell, Depressed cladding, buried waveguide laser formed in a YAG:Nd³⁺ crystal by femtosecond laser writing, *Opt. Lett.* **30**, 2248 (2005).
- [15] N. Sinclair, E. Saglamyurek, M. George, R. Ricken, C. L. Mela, W. Sohler, and W. Tittel, Spectroscopic investigations of a Ti:Tm:LiNbO₃ waveguide for photon-echo quantum memory, *Journal of Luminescence* **130**, 1586 (2010).
- [16] E. Saglamyurek, N. Sinclair, J. Jin, J. A. Slater, D. Oblak, F. Bussi eres, M. George, R. Ricken, W. Sohler, and W. Tittel, Broadband waveguide quantum memory for entangled photons, *Nature* **469**, 512 (2011).
- [17] S. Marzban, J. G. Bartholomew, S. Madden, K. Vu, and M. J. Sellars, Observation of photon echoes from evanescently coupled rare-earth ions in a planar waveguide, *Phys. Rev. Lett.* **115**, 013601 (2015).
- [18] G. Corrielli, A. Seri, M. Mazzera, R. Osellame, and H. de Riedmatten, Integrated optical memory based on laser-written waveguides, *Phys. Rev. Applied* **5**, 054013 (2016).
- [19] C. Liu, T.-X. Zhu, M.-X. Su, Y.-Z. Ma, Z.-Q. Zhou, C.-F. Li, and G.-C. Guo, On-demand quantum storage of photonic qubits in an on-chip waveguide, *Phys. Rev. Lett.* **125**, 260504 (2020).
- [20] S. Wang, L. Yang, M. Shen, W. Fu, Y. Xu, R. L. Cone, C. W. Thiel, and H. X. Tang, Er : linbo₃ with high optical coherence enabling optical thickness control, *Phys. Rev. Applied* **18**, 014069 (2022).
- [21] A. I. Lvovsky, B. C. Sanders, and W. Tittel, Optical quantum memory, *Nat. photonics* **3**, 706 (2009).
- [22] K. Hammerer, A. S. S orensen, and E. S. Polzik, Quantum interface between light and atomic ensembles, *Rev. Mod. Phys.* **82**, 1041 (2010).
- [23] W. Tittel, M. Afzelius, T. Chaneli ere, R. Cone, S. Kr oll, S. Moiseev, and M. Sellars, Photon-echo quantum memory in solid state systems, *Laser & Photonics Reviews* **4**, 244 (2010).
- [24] F. Bussi eres, N. Sangouard, M. Afzelius, H. de Riedmatten, C. Simon, and W. Tittel, Prospective applications of optical quantum memories, *Journal of Modern Optics* **60**, 1519 (2013), <https://doi.org/10.1080/09500340.2013.856482>.
- [25] K. Heshami, D. G. England, P. C. Humphreys, P. J. Bustard, V. M. Acosta, J. Nunn, and B. J. Sussman, Quantum memories: emerging applications and recent advances, *J. Mod. Opt.* **63**, 2005 (2016).
- [26] T. Chaneli ere, G. H et et, and N. Sangouard, Quantum optical memory protocols in atomic ensembles, in *Advances In Atomic, Molecular, and Optical Physics*, Vol. 67, edited by E. Arimondo, L. F. DiMauro, and S. F. Yelin (Academic Press, 2018) Chap. 2, pp. 77–150.
- [27] S. Wehner, D. Elkouss, and R. Hanson, Quantum internet: A vision for the road ahead, *Science* **362**, eaam9288 (2018), <https://www.science.org/doi/pdf/10.1126/science.aam9288>.
- [28] J. Wang, F. Sciarrino, A. Laing, and M. G. Thompson, Integrated photonic quantum technologies, *Nature Photonics* **14**, 273 (2020).
- [29] F. Kaneda, F. Xu, J. Chapman, and P. G. Kwiat, Quantum-memory-assisted multi-photon generation for efficient quantum information processing, *Optica* **4**, 1034 (2017).
- [30] C. W. Thiel, Y. Sun, R. M. Macfarlane, T. B ottger, and R. L. Cone, Rare-earth-doped LiNbO₃ and KTiOPO₄(KTP) for waveguide quantum memories, *Journal of Physics B: Atomic, Molecular and Optical Physics* **45**, 124013 (2012).
- [31] E. Saglamyurek, J. Jin, V. B. Verma, M. D. Shaw, F. Marsili, S. W. Nam, D. Oblak, and W. Tittel, Quantum storage of entangled telecom-wavelength photons in an erbium-doped optical fibre, *Nature Photonics* **9**, 83 (2015).
- [32] C. Liu, Z.-Q. Zhou, T.-X. Zhu, L. Zheng, M. Jin, X. Liu, P.-Y. Li, J.-Y. Huang, Y. Ma, T. Tu, T.-S. Yang, C.-F. Li, and G.-C. Guo, Reliable coherent optical memory based on a laser-written waveguide, *Optica* **7**, 192 (2020).
- [33] A. Seri, G. Corrielli, D. Lago-Rivera, A. Lenhard, H. de Riedmatten, R. Osellame, and M. Mazzera, Laser-written integrated platform for quantum storage of heralded single photons, *Optica* **5**, 934 (2018).
- [34] M. F. Askarani, M. G. Puigibert, T. Lutz, V. B. Verma, M. D. Shaw, S. W. Nam, N. Sinclair, D. Oblak, and W. Tittel, Storage and reemission of heralded telecommunication-wavelength photons using a crystal waveguide, *Phys. Rev. Applied* **11**, 054056 (2019).
- [35] C. Liu, T.-X. Zhu, M.-X. Su, Y.-Z. Ma, Z.-Q. Zhou, C.-

- F. Li, and G.-C. Guo, On-demand quantum storage of photonic qubits in an on-chip waveguide, *Phys. Rev. Lett.* **125**, 260504 (2020).
- [36] A. Seri, D. Lago-Rivera, A. Lenhard, G. Corrielli, R. Osellame, M. Mazzera, and H. de Riedmatten, Quantum storage of frequency-multiplexed heralded single photons, *Phys. Rev. Lett.* **123**, 080502 (2019).
- [37] S. A. Moiseev and S. Kröll, Complete reconstruction of the quantum state of a single-photon wave packet absorbed by a doppler-broadened transition, *Phys. Rev. Lett.* **87**, 173601 (2001).
- [38] B. Kraus, W. Tittel, N. Gisin, M. Nilsson, S. Kröll, and J. I. Cirac, Quantum memory for nonstationary light fields based on controlled reversible inhomogeneous broadening, *Phys. Rev. A* **73**, 020302 (2006).
- [39] M. Afzelius, C. Simon, H. de Riedmatten, and N. Gisin, Multimode quantum memory based on atomic frequency combs, *Phys. Rev. A* **79**, 052329 (2009).
- [40] M. Nilsson, L. Rippe, S. Kröll, R. Klieber, and D. Suter, Hole-burning techniques for isolation and study of individual hyperfine transitions in inhomogeneously broadened solids demonstrated in $\text{pr}^{3+}:\text{Y}_2\text{SiO}_5$, *Phys. Rev. B* **70**, 214116 (2004).
- [41] J. S. Stuart, M. Hedges, R. Ahlefeldt, and M. Sellars, Initialization protocol for efficient quantum memories using resolved hyperfine structure, *Phys. Rev. Res.* **3**, L032054 (2021), arXiv:2103.04581.
- [42] T.-X. Zhu, C. Liu, M. Jin, M.-X. Su, Y.-P. Liu, W.-J. Li, Y. Ye, Z.-Q. Zhou, C.-F. Li, and G.-C. Guo, On-Demand Integrated Quantum Memory for Polarization Qubits, *Phys. Rev. Lett.* **128**, 180501 (2022), arXiv:2201.03691.
- [43] A. Ortu, A. Holzäpfel, J. Etesse, and M. Afzelius, Storage of photonic time-bin qubits for up to 20 ms in a rare-earth doped crystal, *npj Quantum Inf.* **8**, 29 (2022), arXiv:2109.06669.
- [44] S. A. Moiseev and J.-L. L. Gouët, Rephasing processes and quantum memory for light: reversibility issues and how to fix them, *Journal of Physics B: Atomic, Molecular and Optical Physics* **45**, 124003 (2012).
- [45] N. M. Arslanov and S. A. Moiseev, Optimal periodic frequency combs for high-efficiency optical quantum memory based on rare-earth ion crystals, *Quantum Electronics* **47**, 783 (2017).
- [46] M. Sabooni, Q. Li, S. Kröll, and L. Rippe, Efficient Quantum Memory Using a Weakly Absorbing Sample, *Phys. Rev. Lett.* **110**, 133604 (2013).
- [47] E. S. Moiseev, A. Tashchilina, S. A. Moiseev, and B. C. Sanders, Broadband quantum memory in a cavity via zero spectral dispersion, *New Journal of Physics* **23**, 063071 (2021).
- [48] V. Damon, M. Bonarota, A. Louchet-Chauvet, T. Chanelière, and J.-L. L. Gouët, Revival of silenced echo and quantum memory for light, *New Journal of Physics* **13**, 093031 (2011).
- [49] M. M. Minnegaliev, K. I. Gerasimov, T. N. Sabirov, R. V. Urmancheev, and S. A. Moiseev, Implementation of an Optical Quantum Memory Protocol in the $167\text{Er}^{3+}:\text{Y}_2\text{SiO}_5$ Crystal, *JETP Lett.* **115**, 720 (2022).
- [50] S. A. Moiseev, Some general nonlinear properties of photon-echo radiation in optically dense media, *Opt. Spectrosc.* **62**, 180 (1987).
- [51] R. Urmancheev, K. Gerasimov, M. Minnegaliev, T. Chanelière, A. Louchet-Chauvet, and S. Moiseev, Two-pulse photon echo area theorem in an optically dense medium, *Opt. Express* **27**, 28983 (2019).
- [52] S. A. Moiseev, Quantum memory for intense light fields in the photon echo technique, *Bull. Russ. Acad. Sci. Phys.* **68**, 1408 (2004).
- [53] M. M. Minnegaliev, K. I. Gerasimov, R. V. Urmancheev, A. M. Zheltikov, and S. A. Moiseev, Linear stark effect in $\text{Y}_3\text{Al}_5\text{O}_{12}:\text{tm}^{3+}$ crystal and its application in the addressable quantum memory protocol, *Phys. Rev. B* **103**, 174110 (2021).
- [54] D. Roy, C. M. Wilson, and O. Firstenberg, Colloquium: Strongly interacting photons in one-dimensional continuum, *Rev. Mod. Phys.* **89**, 021001 (2017).
- [55] K. H., "Theory of Optical Waveguides", in "Guided-Wave Optoelectronics" (Springer-Verlag, Berlin, 1988).
- [56] D. Walls and G. Milburn, *Quantum Optics*, SpringerLink: Springer e-Books (Springer Berlin Heidelberg, 2008).
- [57] G. L. Lamb, Analytical descriptions of ultrashort optical pulse propagation in a resonant medium, *Rev. Mod. Phys.* **43**, 99 (1971).
- [58] K. Okamoto, *Fundamentals of optical waveguides* (Elsevier, 2021).
- [59] W. B. Mims, Phase memory in electron spin echoes, lattice relaxation effects in CaWO_4 : Er, ce, mn, *Phys. Rev.* **168**, 370 (1968).
- [60] R. L. Cone and G. K. Liu, Power-dependent photon echo decay due to 'instantaneous diffusion' in $\text{tb}^{3+}:\text{LiYF}_4$, *Bull. Am. Phys. Soc.* **33**, 676 (1988).
- [61] C. W. Thiel, R. M. Macfarlane, Y. Sun, T. Böttger, N. Sinclair, W. Tittel, and R. L. Cone, Measuring and analyzing excitation-induced decoherence in rare-earth-doped optical materials, *Laser Physics* **24**, 106002 (2014).
- [62] A. V. Gorshkov, A. André, M. Fleischhauer, A. S. Sørensen, and M. D. Lukin, Universal approach to optimal photon storage in atomic media, *Phys. Rev. Lett.* **98**, 123601 (2007).
- [63] S. A. Moiseev, V. F. Tarasov, and B. S. Ham, Quantum memory photon echo-like techniques in solids, *Journal of Optics B: Quantum and Semiclassical Optics* **5**, S497 (2003).
- [64] E. S. Moiseev and S. A. Moiseev, Scalable time reversal of raman echo quantum memory and quantum waveform conversion of light pulse, *New Journal of Physics* **15**, 105005 (2013).
- [65] G. T. Campbell, O. Pinel, M. Hosseini, T. C. Ralph, B. C. Buchler, and P. K. Lam, Configurable unitary transformations and linear logic gates using quantum memories, *Phys. Rev. Lett.* **113**, 063601 (2014).
- [66] S. E. Beavan, M. P. Hedges, and M. J. Sellars, Demonstration of photon-echo rephasing of spontaneous emission, *Phys. Rev. Lett.* **109**, 093603 (2012).
- [67] E. S. Moiseev, A. Tashchilina, S. A. Moiseev, and A. I. Lvovsky, Darkness of two-mode squeezed light in lambda-type atomic system, *New Journal of Physics* **22**, 013014 (2020).
- [68] N. Skryabin, A. Kalinkin, I. Dyakonov, and S. Kulik, Femtosecond laser written depressed-cladding waveguide 2×2 , 1×2 and 3×3 directional couplers in $\text{Tm}^{3+}:\text{YAG}$ crystal, *Micromachines* **11**, 10.3390/mi11010001 (2020).
- [69] S. A. Moiseev and M. I. Noskov, The possibilities of the quantum memory realization for short pulses of light in the photon echo technique, *Laser Physics Letters* **1**, 303 (2004).
- [70] F. T. Hioe, Solution of bloch equations involving ampli-

- tude and frequency modulations, Phys. Rev. A **30**, 2100 (1984).
- [71] M. M. Minnegaliev, I. V. Dyakonov, K. I. Gerasimov, A. A. Kalinkin, S. P. Kulik, S. A. Moiseev, M. Y. Saygin, and R. V. Urmancheev, Observation and investigation of narrow optical transitions of ^{167}Er ions in femtosecond laser printed waveguides in LiYF crystal, Laser Physics Letters **15**, 045207 (2018).
- [72] J. Dajczgewand, R. Ahlefeldt, T. Böttger, A. Louchet-Chauvet, J.-L. Le Gouët, and T. Chanelière, Optical memory bandwidth and multiplexing capacity in the erbium telecommunication window, New Journal of Physics **17**, 023031 (2015).